FREE-TO-ROLL STUDY OF UNCOMMANDED LATERAL MOTIONS FOR THE VENTED STRAKE F/A-18E/F

By

Elaine Melendez Bryant

Thesis submitted to the Faculty of the Graduate School of the
University of Maryland, College Park, in partial fulfillment
of the requirements for the degree of
Master of Science in
Aerospace Engineering
2005

Advisory Committee:
Professor Jewel Barlow, Chair
Professor Emeritus John Anderson
Dr. D. Bruce Owens

APR 11 2005

REPORT DOCUMENTATION PAGE

Form Approved
OMB No. 0704-0188

1. AGENCY USE ONLY *(Leave blank)*	2. REPORT DATE	3. REPORT TYPE AND DATES COVERED
	7.Apr.05	THESIS

4. TITLE AND SUBTITLE
FREE-TO-ROLL STUDY OF UNCOMMANDED LATERAL MOTIONS FOR THE VENTED STRAKE F/A-18E/F

5. FUNDING NUMBERS

6. AUTHOR(S)
CAPT BRYANT ELAINE M

7. PERFORMING ORGANIZATION NAME(S) AND ADDRESS(ES)
UNIVERSITY OF MARYLAND AT COLLEGE PARK

8. PERFORMING ORGANIZATION REPORT NUMBER

CI04-1030

9. SPONSORING/MONITORING AGENCY NAME(S) AND ADDRESS(ES)
THE DEPARTMENT OF THE AIR FORCE
AFIT/CIA, BLDG 125
2950 P STREET
WPAFB OH 45433

10. SPONSORING/MONITORING AGENCY REPORT NUMBER

11. SUPPLEMENTARY NOTES

12a. DISTRIBUTION AVAILABILITY STATEMENT
Unlimited distribution
In Accordance With AFI 35-205/AFIT Sup

DISTRIBUTION STATEMENT A
Approved for Public Release
Distribution Unlimited

12b. DISTRIBUTION CODE

13. ABSTRACT *(Maximum 200 words)*

14. SUBJECT TERMS

15. NUMBER OF PAGES
61

16. PRICE CODE

17. SECURITY CLASSIFICATION OF REPORT	18. SECURITY CLASSIFICATION OF THIS PAGE	19. SECURITY CLASSIFICATION OF ABSTRACT	20. LIMITATION OF ABSTRACT

ABSTRACT

Title: Free-to-Roll Study of Uncommanded Lateral
                                Motions for the Vented Strake F/A-18E/F

                                Elaine Melendez Bryant, Master of Science,
                                2005

Directed By: Dr. Jewel Barlow, Department of Aerospace

                                Engineering

A free-to-roll study was conducted on the lateral characteristics of a 10% scale model

pre-production vented strake F/A-18E/F. This study carried out both static force and

moment tests along with free-to-roll tests to determine the correlation to previous

studies, assess the lateral motion, and verify free-to-roll as a viable test technique for

the determination of uncommanded lateral motion potential. Static force and moment

tests established correlation with previous studies. Using a figure of merit, the free-

to-roll tests captured the angle of attack range over which the wing drop occurred in

flight tests. Based on the equation of motion, the possible contributors to the lateral

motion were: the character of the forcing function, the static lateral stability and roll

damping. To determine the causal contributions three different angles of attack were

analyzed, verifying the importance of free-to-roll as a viable test technique when used

in conjunction with static test results.

Dedication

MI FAMILIA

Acknowledgements

There are many people that have gotten me to this point and I would like to acknowledge all of them:

- I thank God for his many blessings, his inspirations and love

- My husband, ███, who supported me throughout this 18-month journey. I could not have done it without you.

- My parents who sacrificed so much for my education. I am forever grateful.

- My sisters, ███ and ███, for keeping me sane and always making me laugh.

- To the Air Force for giving me the opportunity to continue my education at an excellent institution, the University of Maryland.

- Thanks to my advisor Dr. Barlow for inspiring this work and letting it take flight.

- Thanks to Steve Cook and Steve Donaldson from NAVAIR and the Navy for helping to get this project started with NASA.

- Many thanks to the Flight Dynamics Branch at NASA Langley for sponsoring the project via use of the 12-Foot Tunnel and the valuable technician time of Wes O'Neal, Earl Harris and Gary Bayless.

- A very special thanks to Dr. Bruce Owens for jumping head first into this project and for all his support during the testing, analysis and writing of this thesis.

- I would like to thank all those past and present that have inspired me to continue my aerospace education: Dr. Tom Yechout, Dr. George Havener, and Dr. John Anderson.

Table of Contents

List of Figures

List of Symbols and Abbreviations

α angle of attack

Δ change

ρ density

ϕ roll angle

$\dot{\phi}$ roll rate, the time derivative of roll angle

$\ddot{\phi}$ roll acceleration, time derivative of roll rate

A/C   aircraft

AIL   ailerons

AWS   Abrupt Wing Stall

b   reference wing span

CFD   computational fluid dynamics

C_l, Cl   rolling moment coefficient

C_{lo} aerodynamic forcing function

$C_{l\phi}$ $\dfrac{\partial C_l}{\partial \phi}$, partial derivative, static lateral stability

$C_{l\dot{\phi}}$ $\dfrac{\partial C_l}{\partial \left(\dfrac{\dot{\phi} b}{2V_\infty} \right)}$, partial derivative, roll damping coefficient

C_{lp} $\dfrac{\partial C_l}{\partial \left(\dfrac{p b}{2V_\infty} \right)}$, partial derivative, roll damping coefficient

Note: $C_{l\dot{\phi}}$ and C_{lp} are kinematically equivalent [9]

Fr#   Froude number

ft   foot/feet

FOM   Figure of Merit

FTR   free-to-roll

g   acceleration due to gravity

HT   horizontal tail

I   inertia

I_x inertia about the roll axis

l   characteristic length

LE   leading edge

LEX   leading edge extension

m   model

n   scale factor

NASA   National Aeronautics and Space Administration

P_{P-V} free-to-roll figure of merit

psi   pounds per square inch

q   dynamic pressure

Re#   Reynolds number

S   reference surface area

s   seconds

t   time

TEF   trailing edge flaps

V   wind tunnel velocity

V_∞ free stream velocity

VT   vertical tail

1 Introduction

1.1 F/A-18E/F Background

1.1.1 The Navy's Premier Fighter

The Navy's newest fighter is the F/A-18E/F Super Hornet. In operation since November 1999 it is a premier strike fighter made to be tough, flexible and survivable for the missions and demands of today's Navy. The F/A-18E is the single seat model and the F model has two seats. To meet the demands of naval and maritime warfare the F/A-18E/F has eleven weapons stations capable of carrying both air-to-air and air-to-ground precision guided weapons. Two General Electric F414-GE-400 engines capable of producing 44,000 lbs of thrust power the F/A-18E/F. Advanced aerodynamic designs have maximized the combat maneuverability and usable angle of attack while increasing the resistance to spins. The F/A-18E/F is capable of carrying out numerous missions including: air superiority, day and night strike, fighter escort, close air support, suppression of enemy air defenses, maritime reconnaissance, forward air control and tanker missions [7]. Figure 1-1 shows the F/A-18E/F in action performing a carrier landing onto the USS Abraham Lincoln.
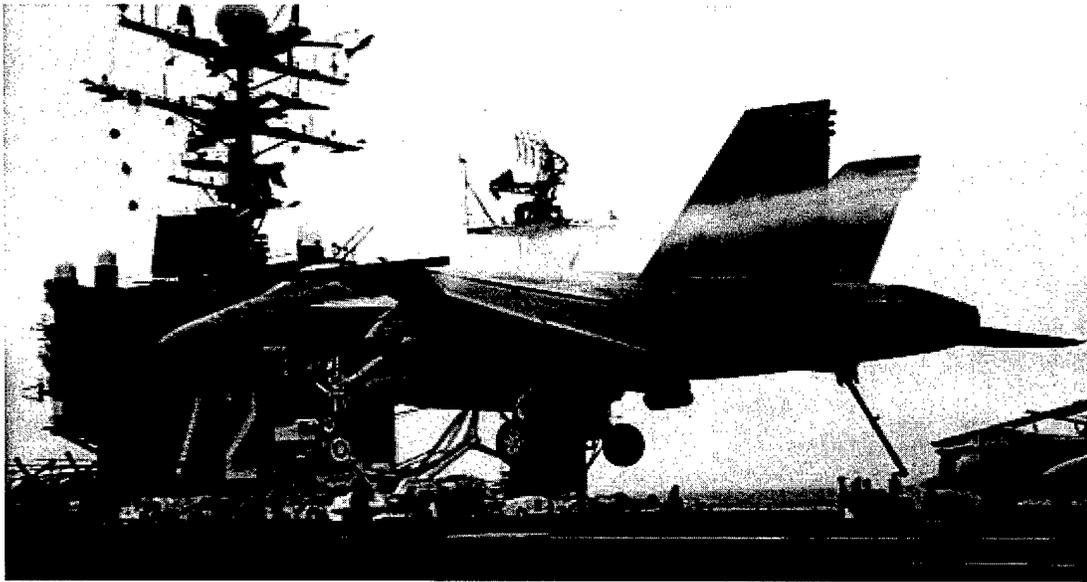
Figure 1-1: The F/A-18 landing on the USS Abraham Lincoln [7]

1.1.2 The Pre-production Model

January 1988 marked the beginning of the road to operational status for the F/A-18. What began as a concept for the Hornet 2000 developed into an on-time and on-weight project showcasing advancements in pre-production engineering. One of the pre-production designs of the F/A-18 included vented strakes or vented Leading Edge Extensions (LEX). The LEX extended from a midpoint on the fuselage to the wing Leading Edge (LE) and was designed to produce vertical lift at angles of attack larger than wing stall [3]. The LEX vents were located where the LEX met the LE above and just to the outside of the intake (See Figure 1-2). The purpose of the LEX vents was to increase maneuverability and to reduce buffeting of the vertical tails. In addition to these design benefits wind tunnel tests showed that opening the vents improved high speed turn performance and lift performance at angles of attack higher than design approach angles

[3]. Figure 1-2 shows the pre-production model with the LEX vents in the open position. The vents are in the closed position when they are flush with the LE and the LEX.
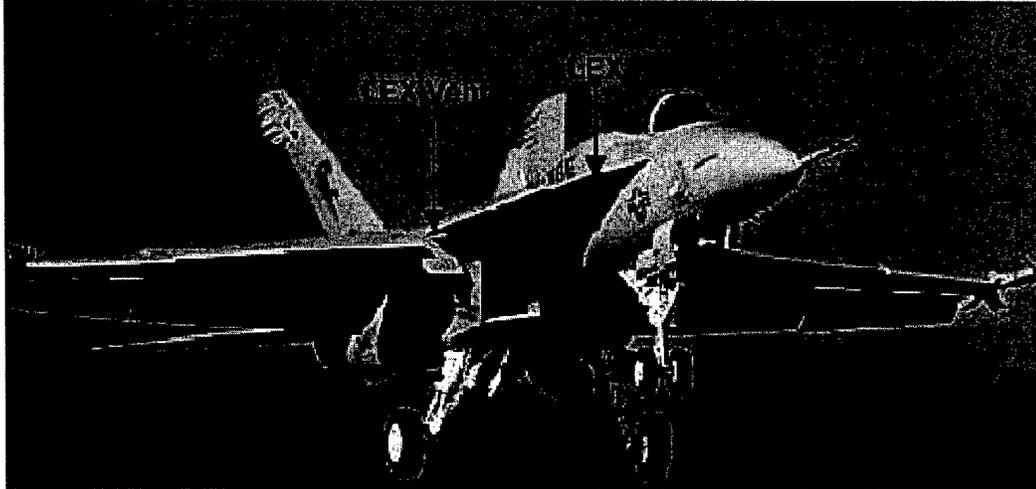
Figure 1-2: Pre-production F/A-18E/F with LEX Vents in the Open Position [3]

1.1.3 Flight Tests

In 1996, flight tests were performed with the LEX vents in the open position. One of the configurations tested was the Powered Approach (PA), which consisted of landing gear down, the LE set as a function of the angle of attack, the ailerons (AIL) drooped symmetrically at 40° and the trailing edge flaps (TEF) set at 40°. The flight tests were also conducted using a PA-half configuration, which was the same as the PA except the AIL and TEF were set at 30°. During these flight tests uncommanded lateral motions were detected when the vents were open for both the PA and the PA-half. Figure 1-3 shows the results from several of the flight tests. The uncommanded lateral motions, or wing drop, were unpredictable and occurred at angles of attack between 12° and 16°. In all there were 30 occurrences of wing drop during the flight tests and after careful evaluation it was determined that opening the vents was the cause. In addition, flight test data showed that the benefits for which the vents were designed were not manifesting

3

themselves [3]. Due to the flight safety risk the LEX vents were permanently closed and thus the wing drop issue was eliminated from the operational F/A-18 Super Hornet.

Aircraft, Flight, and Maneuver	Angle of Attack (deg)	Angle of Sideslip (deg)	Leading Edge Flap Position (deg)	Trailing Edge Flap Position (deg)
E1, 12, 19	15.0	0.0	30	40
E2, 17, 67	12.1	-0.4	26	40
E1, 26, 18	15.8	0.2	30	30
E1, 26, 20	15.0	0.7	30	40
E2, 39, 13	14.5	0.5	28	40
E2, 39, 21	13.6	-2.5	15	30
E2, 39, 23	13.8	1.2	15	40
E2, 39, 24	13.7	0.0	15	40
E2, 40, 41	13.3	-1.2	27	40
F1, 06, 12	14.2	Not available²	28	40

Figure 1-3: Results from Several Pre-production In-Flight Tests [3]

1.2 Previous Studies

1.2.1 Bifurcation Phenomenon

Although closing the LEX vents eliminated the wing drop problem, questions remained as to the occurrence and cause of the wing drop and how the vents open configuration played a roll. Several studies have been done to investigate this problem including one by Ericsson. He concluded that wing-body rock originates from vortex shedding emanating from the forebody [4]. In 1999 Steve Cook conducted an in-depth study into the behavior of the flow over the F/A-18. He determined that the phenomenon was characteristic of a subcritical flow bifurcation, "the abrupt replacement of an unstable flow topology with a stable one"[3]. A bifurcation is the change in quality of the flow due to the change in some physical parameter [8]. In the case of F/A-18, the parameter was angle of attack. Such bifurcations have been identified over circular cylinders, slender bodies and symmetric aircraft [1,3,11]. Cook concluded from flow visualization

tests that opening the vents lifted the vortices coming off the strakes away from the wing surface and pushed them toward the fuselage [3]. The result was a separated region at mid wing that grew with increasing angle of attack. Once a particular angle of attack is reached, the separated region affects the outboard portion of the wing causing a loss of lift. Due to the unpredictable nature of the bifurcation, this can occur asymmetrically, hence the wing drop.

1.2.2 Static Force and Moment Test

Cook conducted static force and moment tests as part of his in-depth study [3]. The data revealed that specific aerodynamic parameters or state variables were associated with the bifurcation. The set of variables for which the bifurcation occurs is called the critical state. Cook's experiments matched the literature done by G. F. Moss, which indicated that, a reflex or spike in the plots of the aerodynamic parameters were indications of a critical state and therefore the occurrence of a bifurcation [3]. Cook's data showed that the bifurcation occurred at approximately 16° angle of attack. Figure 1-4 shows the results of one of his tests. The arrows were added to indicate the spikes and reflexes in the particular curves.
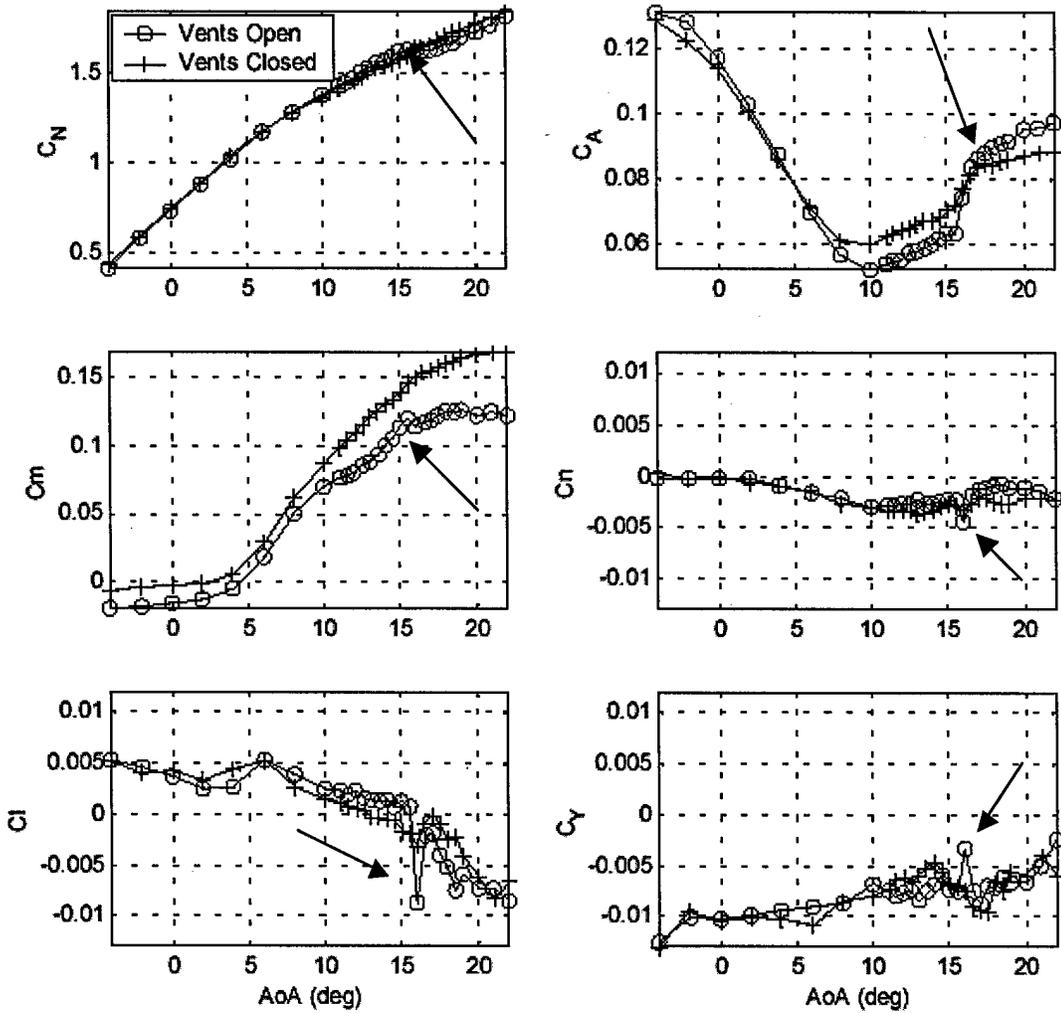
Figure 1-4: Results from Cook [3], "Effect of LEX vent deflection on F/A-18E configuration, LEF=10°, TEF=30°, and AIL=30°"

Cook's results showed that an angle of attack of 16° was a critical state. This angle of attack falls within the range of angles of attack seen in the flight tests.

1.2.3 Computational Fluid Dynamics

Filbey and Niewoehner, test pilot for the pre-production F/A-18, conducted a Computational Fluid Dynamics (CFD) study into the lateral instabilities observed in flight using a half plane model [5]. The computational results matched those of Cook [3] identifying a wing drop between 15°and 16° angle of attack.

6

1.2.4 Transonic Free-to-Roll Test

In parallel with the static wind tunnel testing and the computational work, a study was conducted to look into the occurrence of Abrupt Wing Stall (AWS) at transonic speeds for the F/A-18. The AWS program conducted by NASA with collaboration from other agencies shed light on the occurrence of wing drops at transonic speeds. One of the test techniques used was Free-to-Roll (FTR). In contrast to the static wind tunnel tests and the CFD, the FTR test allowed for the study of the dynamic behavior of the lateral motions. Owens et al. provide a detailed description of the FTR setup and validate FTR as a viable test technique for the identification of uncommanded lateral motions on four different aircraft, including the pre-production F/A-18 at the transonic range [9]. One of the main benefits of the FTR tests is that it allows for the analysis of lateral activity including roll damping. This type of analysis proved vital in characterizing and explaining the causes for uncommanded lateral motions in the transonic range.

1.3 Motivation/Objectives

Based on the findings from the static testing, the CFD, and the FTR testing at transonic speeds, it was of interest to evaluate the feasibility of detecting the potential for uncommanded lateral motions (wing drop or abrupt wing stall) at subsonic speeds for the F/A-18E with the vents open. The main objectives were as follows:

1.3.1 Correlation

Conduct static force and moment tests using a 10% scale model of the F/A-18E to determine the correlation between the previous static tests, the CFD and most importantly

the flight test data. In addition, it was hoped that the static tests would provide a range of angle of attack to focus the FTR testing.

1.3.2 Lateral Motion Assessment

Conduct a FTR study on the same model and assess the lateral characteristics including the unsteady aerodynamics and roll damping to gain understanding into the dynamic motions that may be contributing to wing drop.

1.3.3 Feasibility

Determine if FTR testing is a viable technique for the determination of the potential for uncommanded lateral motions at subsonic speeds for the pre-production F/A-18E. Other studies such as Raj et al. have determined the importance of integrating methods such as static force, moment testing and CFD [10]. This study will determine the feasibility of FTR when used in conjunction with static force and moment data.

8

2 Experimental Approach

2.1 Test Overview

2.1.1 Wind Tunnel Description and Test Conditions

Both the static and the FTR tests were conducted at the NASA Langley 12-Foot Low-Speed Tunnel in Hampton VA. The tunnel is closed circuit with a 12 ft octagonal-test section and can reach speeds up to 77 $\frac{ft}{s}$. The Reynolds number range is 0 to 0.5 x 10^6/ft. The facility provides the capability to test using sting mounted models with internal balances. For this study the tunnel was run at a dynamic pressure (q) of 4 $\frac{lb}{ft^2}$, due to structural limitations on the model.

$$q = \frac{1}{2}\rho V^2 \qquad \textbf{Dynamic Pressure} \qquad\qquad \textbf{Equation 2-1}$$

$$V = \sqrt{\frac{2q}{\rho}} \qquad \textbf{Tunnel Velocity} \qquad\qquad \textbf{Equation 2-2}$$

$$RE\# = \frac{\rho Vl}{\mu} \qquad \textbf{Reynolds Number} \qquad\qquad \textbf{Equation 2-3}$$

Using sea level density and chord length as the characteristic length, the tunnel velocity was 58 $\frac{ft}{s}$ and the Reynolds number was calculated to be 498,748 or approximately 0.5 x 10^6.

2.1.2 Model Description and Configurations

The model used was a 10% scale model of the pre-production F/A-18E. The model was made of balsa wood, fiberglass, plywood and aluminum and it was equipped with wing tip missiles, canopy, LEF, AIL, flap shrouds, TEF, Vertical Tails (VT), Horizontal Tail (HT) and LEX vents. All the control surfaces were variable and could be set to specific values. The control surface settings for this experiment were consistent with a PA-half configuration; LE set at 10° and TEF and AIL set at 30°. This is the same model that Cook [3] used in his study also conducted at the NASA 12-Foot Tunnel. Because of the FTR, testing some internal modifications were made to accommodate the static force, moment balance and the FTR mount. The various configurations used were vents open and vents closed, VT on and VT off. Figure 2-1 shows the 10% scale model in the 12-Foot Tunnel.
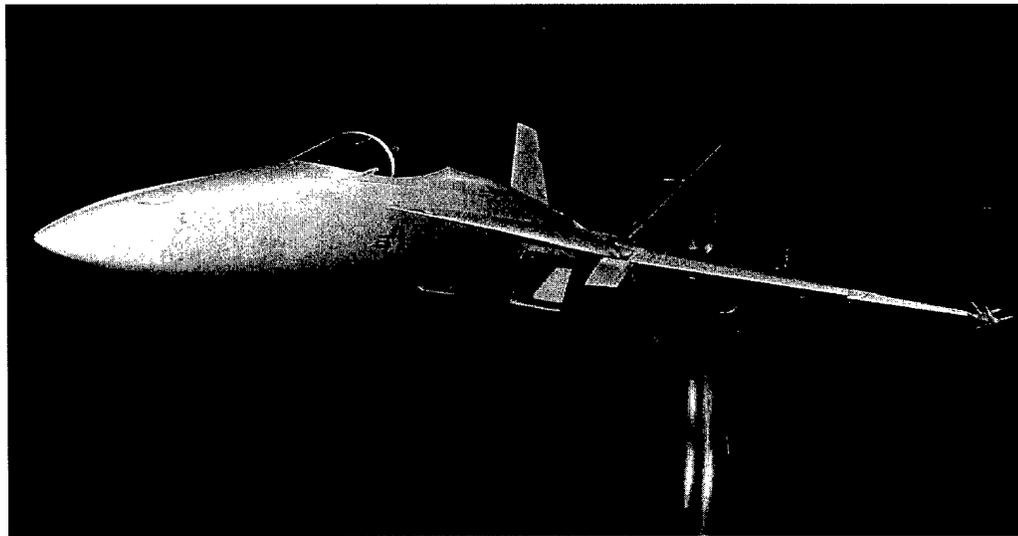
Figure 2-1: 10% Scale F/A-18 in the NASA Langley 12-Foot Tunnel

2.1.3 Dynamic Scaling

Dynamic scaling ensures that the results of the scale model test can be applied to a full-scale aircraft. Two flows are dynamically scaled or similar if the streamlines are geometrically the same and the coefficients of force are the same [1]. Wolowicz describes several similitude parameters that must be considered for dynamic scaling: geometric configuration, angle of attack, Reynolds number, Mach number, Froude number, and inertia scaling [12]. The 10% scale model is geometrically similar to the full scale F/A-18E/F. The angles of attack used in the testing matched those for wing drop occurrence in flight tests.

Ideally the test Reynolds number should not be lower than that in flight otherwise the ratio of inertia forces to viscous forces is lower and it negates dynamic scaling [12]. However, due to wind tunnel and model size restrictions the Reynolds number is typically lower for most wind tunnel tests. The scaling factor for Reynolds number is $\frac{Re\#m}{Re\#A/C}n = 1$, where n is the model-scaling factor, m stands for model and A/C is for the aircraft [12]. For this test n=1/10, the model Reynolds number in the wind tunnel is 0.5×10^6 and the flight Reynolds number is 1.94×10^7. Given the approach speed of the F/A-18E is $226\frac{ft}{s}$ [6], the flight Reynolds number is larger than the wind tunnel model and the right hand side of the equation is 0.002 instead of 1.

Since the Mach numbers of the wind tunnel test (.051) and flight (.202) are less than 0.3 the flow is assumed incompressible (i.e. compressibility effects are negligible). Mach number scaling is not crucial when dealing with incompressible flow [1].

11

To ensure that inertial and gravitational effects are scaled properly the Froude number for

both the model and aircraft should match [12]. The equation is $Froude\# = \dfrac{V^2}{lg}$, where l is

the characteristic length (span) and g is the acceleration due to gravity. In this test the

model Froude number is 251 and the aircraft Froude number is 382. Inertia scaling goes

hand in hand with Froude number in ensuring inertial and gravitational effects are

similar. The scale factor is $\dfrac{I_m}{I_{A/C}} = \dfrac{\rho_m}{\rho_{A/C}} n^5$, where ρ is the density and I is the inertia.

The full-scale inertia value is approximately 39,000 slug-ft^2 and the model inertia was

experimentally found to be .40 slug-ft^2. Using the above equation it is clear that the

model is close to being inertially scaled.

The fact that the Reynolds number and the Froude numbers are not exactly scaled is

important to note and understand. The nature of the FTR test allows for this discrepancy

because the results are not used to directly predict aircraft motion, but rather tendencies.

2.2 Static Force and Moment Test Setup

2.2.1 Balance Setup and Information

The internally mounted six-component strain gauge balance used for the static force and

moment testing was the NASA FF-12. It is internally mounted along the longitudinal

axis of the model with its moment reference center placed at the center of gravity to

maximize the range on the moment beams. Figure 2-2 shows the bottom view of the

10% scale model revealing the placement along the axis of the balance.
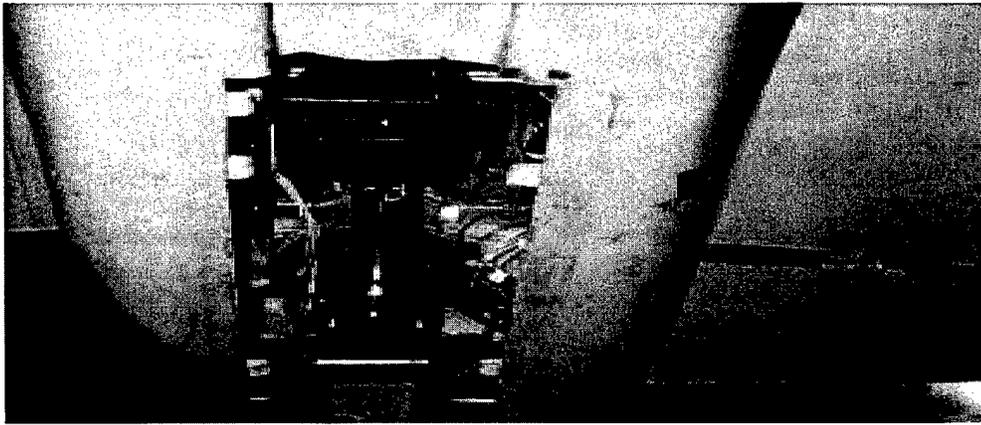
Figure 2-2: Bottom View of Balance Placement Inside the 10% Scale Model

2.2.2 Data Collection and Sampling Frequency

The static data was collected using a 4 Hz filter. Time histories were collected for all the data. Several sampling frequencies were tried in order to determine the best frequency at which to test. Figure 2-3 shows a rolling moment coefficient time history comparison between 10 Hz and 80 Hz sampling frequency. The data for the plot was collected at 10° angle of attack with the vents in the open position. Note that there is no distinct variation between the two time histories. Similar results were seen for the other five force and moment coefficients.
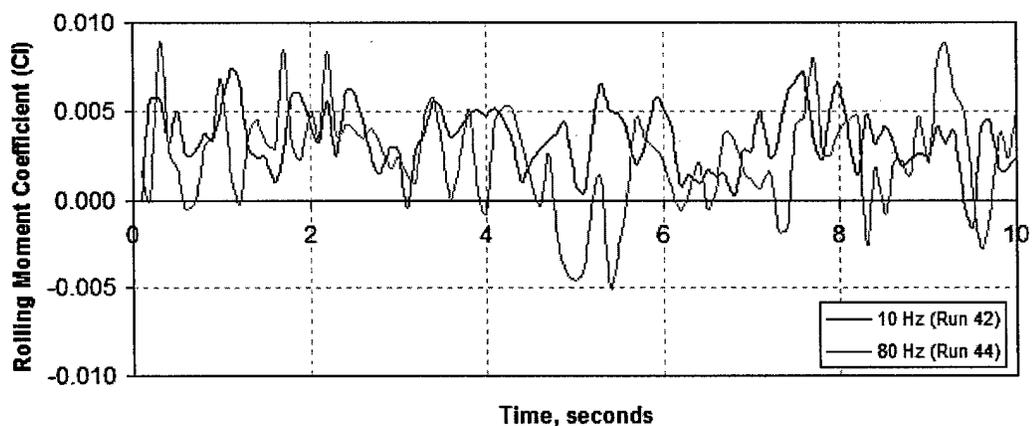
Figure 2-3: Rolling Moment Time History Comparison Between 10 Hz and 80 Hz, Static Data

13

To investigate the variation of the data, the standard deviation was calculated for the various sampling frequencies tested. Figure 2-4 shows a plot of the standard deviations for the various angles of attack. This plot confirms the initial suggestion from Figure 2-3, that there is not much difference in the data when you sample at the various frequencies. Since all four frequencies exhibit fairly small standard deviations, any sampling rate would have sufficed. A sampling frequency of 80 Hz was chosen for this study because it provided a higher sampling frequency without the expense in processing time required to sample at 160 Hz. In addition the 80 Hz sampling rate increased the resolution in order to facilitate a more accurate study of the system unsteadiness.
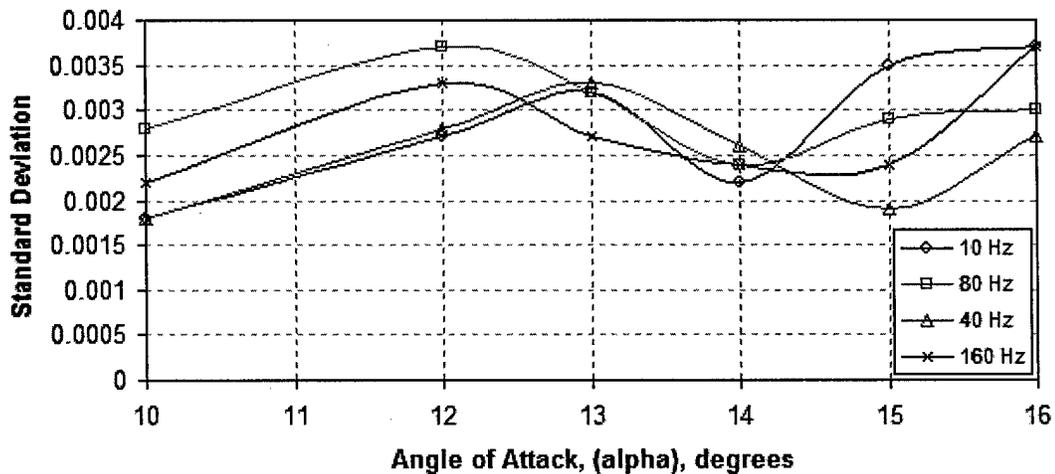
Figure 2-4: Standard Deviation Comparison, Static Data

14

2.3 Free-to-Roll Test Setup

The model is mounted to a rig on a sting, which allows it to move freely along the body axis. Figure 2-5 shows a sketch of the model in the tunnel on the FTR rig.   At wings level the angle of attack and pitch angle are equal and the sideslip value is zero. Both the yaw and pitch angles are fixed. A roll to the right increases the angle of attack seen by the right wing, while decreasing the angle of attack seen by the left wing. The opposite is true for a roll to the left.
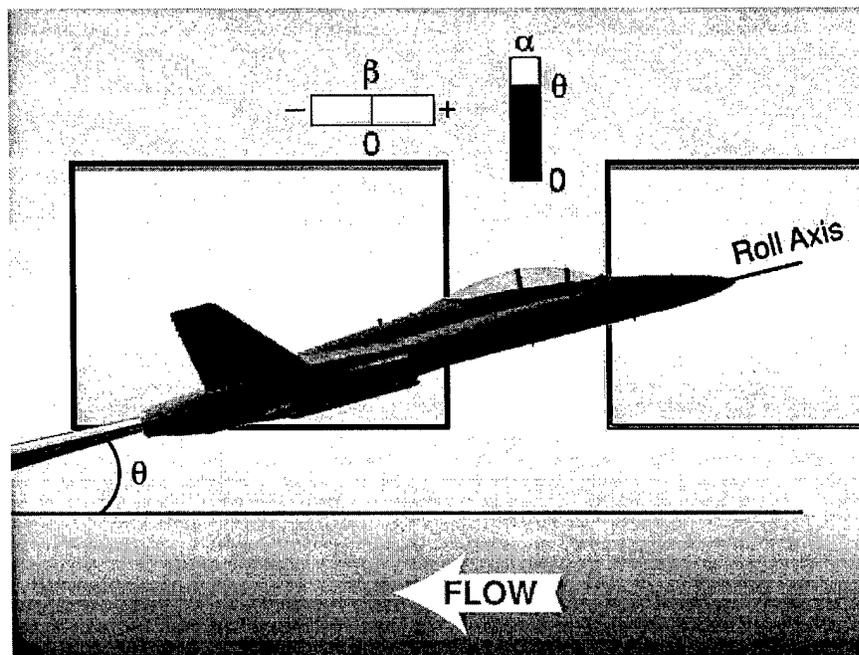
Figure 2-5: Kinematics of FTR Setup

2.3.1 Equation of Motion

The equation of motion for the FTR test is:

$$\frac{I_x \ddot{\phi}}{qSb} + C_{l\dot{\phi}} \frac{\dot{\phi} b}{2V_\infty} + C_{l\phi}\phi = C_{lo} \qquad \text{FTR Equation of Motion} \qquad \textbf{Equation 2-4}$$

15

The equation is analogous to a mass-spring-damper system with a forcing function. The first term on the left hand side of the equation is the mass moment of inertia. It includes the inertia along the roll axis (I_x), dynamic pressure (q), reference surface area (S), reference wing span (b) and the roll acceleration ($\ddot{\phi}$). The roll acceleration is the second time derivative of the roll angle. The roll angle is the data collected from the FTR test. The second term on the left is the roll damping term and it consists of the roll rate ($\dot{\phi}$), b, free stream velocity (V_∞), and the roll damping coefficient ($C_{l\dot{\phi}}$). The third term on the left consists of the partial derivative $C_{l\phi}$, and the roll angle (ϕ). This term represents the static lateral stability or in the case of the mass-spring damper it corresponds to the spring effects. The term on the right hand side of the equation is the aerodynamic forcing function, (C_{lo}). Each one of these terms has a contribution to the motion of the model in the FTR test. It is important to note that all of these contributions are aerodynamically induced and that there is not pilot and/or control system input. For this reason, the results from these tests must be evaluated as open-loop activity and they cannot be used to directly predict aircraft motion.

2.3.2 Free-To-Roll Rig and Brake

The rig used for the FTR test mounts internally to the body on the model's longitudinal body axis. The rig contains two sets of ball bearings, was designed to minimize the addition of roll inertia to the model, and mounts in the same location as the static force and moment balance.

Part of the FTR set up was a brake system that allowed for the model to be held in static condition. Figure 2-6 shows the valving for the brake system. The brake was powered by compressed air at 175 psi and it was essential in attainting the initial conditions.

Figure 2-6: Air Brake System Used For The FTR Testing

2.3.3 Test Points

There were three types of test points used for the FTR test technique. The first was the **continuous pitch sweep**. This involved sweeping the model through a series of pitch angles in order to provide a general assessment for the range of angle of attacks at which the wing drop might occur. The model was brought to wings level at 0° pitch angle, the brake was released, the pitch sweep up to 20° pitch angle and data was recorded. Once at 20° the sequence was repeated with a pitch sweep down to 0° pitch angle.

The second test point used was the **pitch pause**. For this test point the model was first set at wings level using the brake and then moved to the desired pitch angle. The brake was released and data was taken for at least 30 seconds. This test point captured the

lateral activity at a given pitch angle. Note that when the wings are level the pitch angle is equivalent to the angle of attack.

The third and final test point was the **bank and release**. For this point the model was given an initial roll angle and a specific pitch angle, the brake was released and data was taken. This test point was crucial in determining the effects of roll damping on the lateral motion.

2.3.4 Free-to-Roll Figure of Merit

In order to assess the severity of the motion seen in the pitch pause test points, a Figure of Merit (FOM) was used in the analysis process. The FOM used was the same one used in similar FTR tests in the transonic range by Owens et al. [9]. This particular FOM captures both amplitude and rate effects. Figure 2-6 below does not represent actual data from this study but it illustrates the definition of FOM. To calculate the FOM, the difference between each local maximum (peak, P) and each local minimum (valley, V) was calculated for the entire set of data.
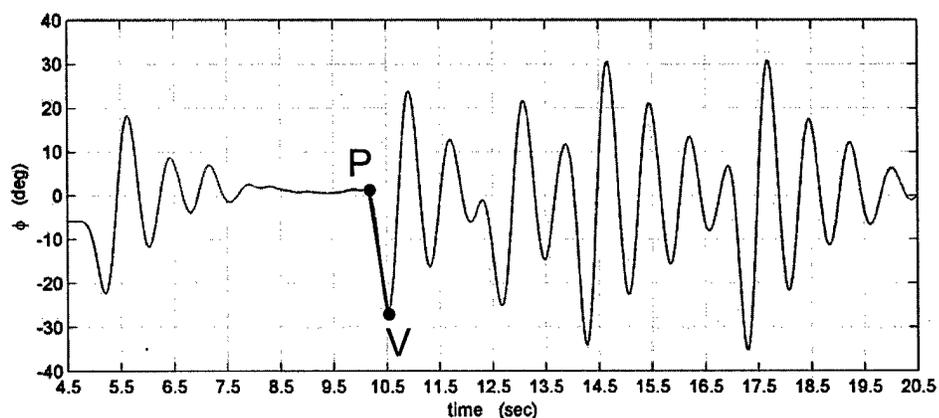

Figure 2-7: Illustration Of FTR FOM [9]

18

Each of these differences is then divided by the time it takes to get from the minimum to the maximum. Each of these ratios is non-dimensionalized and the highest of these values is taken as the FOM. The equation that defines the FTR FOM is:

$$p_{P-V} \equiv \left(\left| \frac{\Delta \phi}{\Delta t} \right| \frac{b}{2V_\infty} \right)_{max}$$ **FTR FOM Definition**   **Equation 2-5**

2.3.5   Miscellaneous Test Information

Flow visualization was attempted during the FTR portion of the test. Several mini-tuft candidates were assessed. One was chosen but after application of the tufts to the entire model it was determined that the fluorescent lighting available at the tunnel facility was not sufficient to illuminate the tufts in a manner that would provide sufficient information on the flow over the model. Video was taken of all the FTR tests. There were two camera views recorded; a top view and a view from the back end of the model. The video allowed for visual assessment of the lateral motions.

3 Experimental Results

3.1 Static Force and Moment Results

3.1.1 Effect of Vertical Tails

To determine if the VT interaction contributed to the wing drop, tests were conducted with and without the VT for the vents closed and the vents open configurations. Figure 3-1 shows that at a low angle of attack of 10°, where wing drop was not observed, there were no significant differences between the VT on and VT off configuration.


(a) Vents Open, Alpha=10 degress

(b) Vents Closed, Alpha=10 degrees
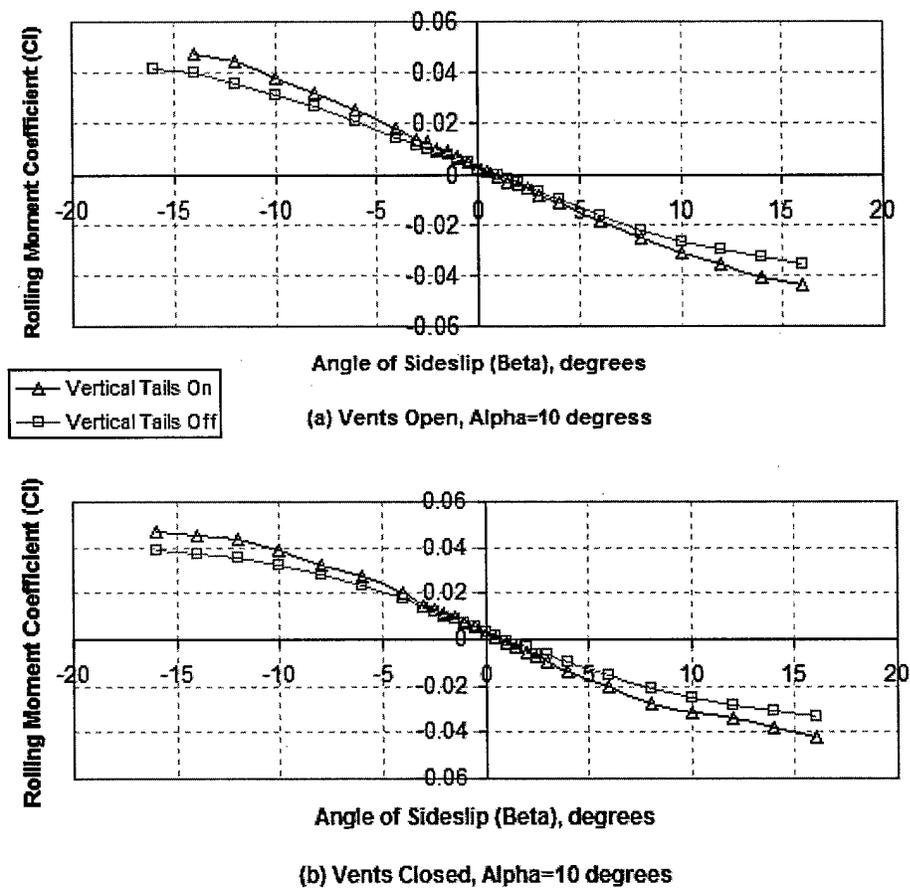
Figure 3-1 (a, b): Effect of Vertical Tail at Angle of Attack 10°

Figure 3-2 shows that at the higher angle of attack of 16°, where wing drop was detected, there was again no significant difference between the VT on and VT off configuration. Note that at this angle of attack the rolling moment coefficient curve is not as smooth as it is at the lower angle of attack, which is indicative of the bifurcation.

(a) Vents Open, Alpha=16 degrees

—△— Vertical Tails On
—□— Veritcal Tails Off

Angle of Sideslip (Beta), degrees

(b) Vents Closed, Alpha=16 degrees
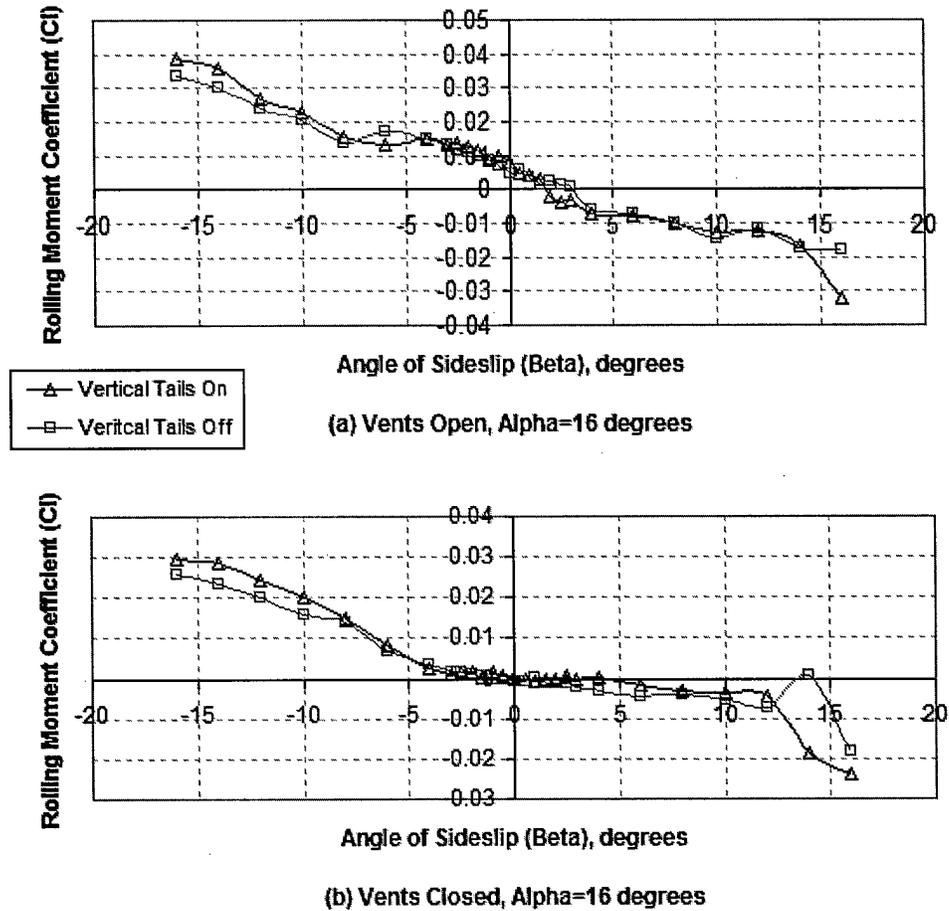
Figure 3-2 (a, b): Effect of Vertical Tail at Angle of Attack 16°

The results in all four graphs indicate that there is no significant difference between the VT on and the VT off configurations and that this is valid only in a sideslip range of –5° to 5°. The data presented in the rest of this paper will be with VT on since the proceeding data falls within the prescribed sideslip range.

3.1.2 Effect of Vent Positioning

The primary concern for this study is the effect of the vent position on the aerodynamic characteristics of the model. The lift curve is of interest because previous studies have indicated that a reflex in this curve is an indication of a bifurcation and hence possibly wing drop [3,8]. Figure 3-3a shows the lift curve slope for the vents open configuration. It is clear that there is a reflex at about 15.5 ° angle of attack, indicated by the arrow in the inset. This is approximately the same angle of attack that Cook [3] identified as a critical state. Figure 3-3b shows the vents closed configuration. Wing drop was not experienced in this configuration and a smooth lift curve with no reflex is a strong indication that no bifurcation exists in this configuration.
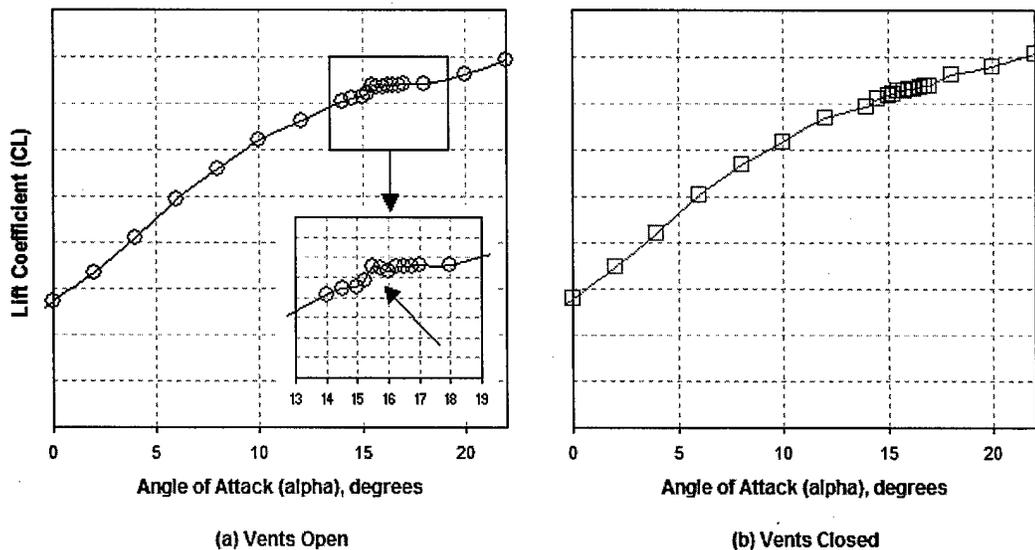

Figure 3-3 (a, b): Lift Curve for the Vents Open and Closed Configurations, Static Data

Based on the results in Figure 3-3 two other test runs were done with finer alpha increments to focus in on the critical state. Figure 3-4 shows that both configurations exhibit some oscillations but the jumps in the vents open configuration are larger and

22

more pronounced than the vents closed configuration. The smaller angle of attack increments show pronounced reflexes at angle of attacks equal to 14.5° and 16.5°. These results although different from the previous plot indicate that there is some propensity for wing drop in the same angle of attack range seen in flight tests [3].
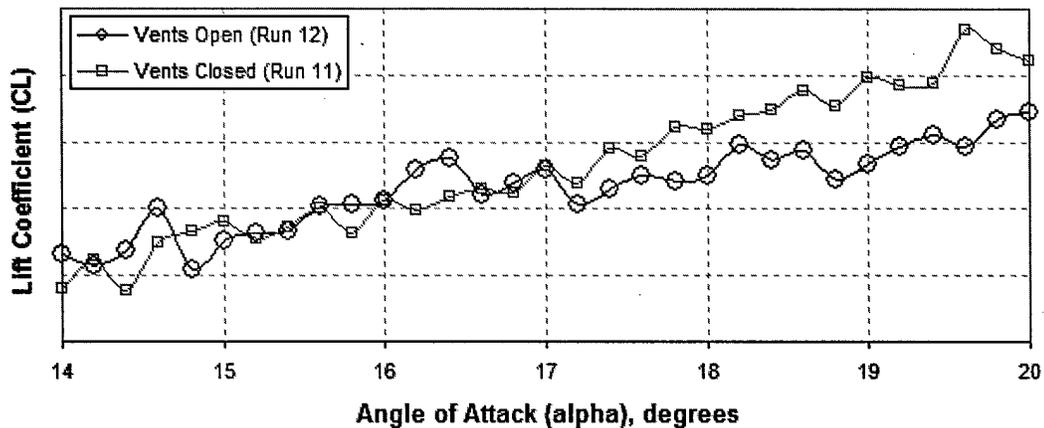

Figure 3-4: Effect of LEX Vent Positioning, Smaller Angle of Attack Increments

In addition to the lift curve slope the other force and moment coefficient data shed light on the existence of a critical state. Figure 3-5 shows angle of attack versus the six force and moment coefficients. The normal force coefficient curve indicates a slope change for the vents open configuration. The top right plot shows that the vents open configuration yields smaller values for axial force coefficient than the vents closed configuration. This is also true for the pitching moment coefficient. Both the yawing moment and rolling moment coefficient curves spike near angle of attack 16°. There is no clear difference in the curves for vents open and closed in the side force coefficient.

23
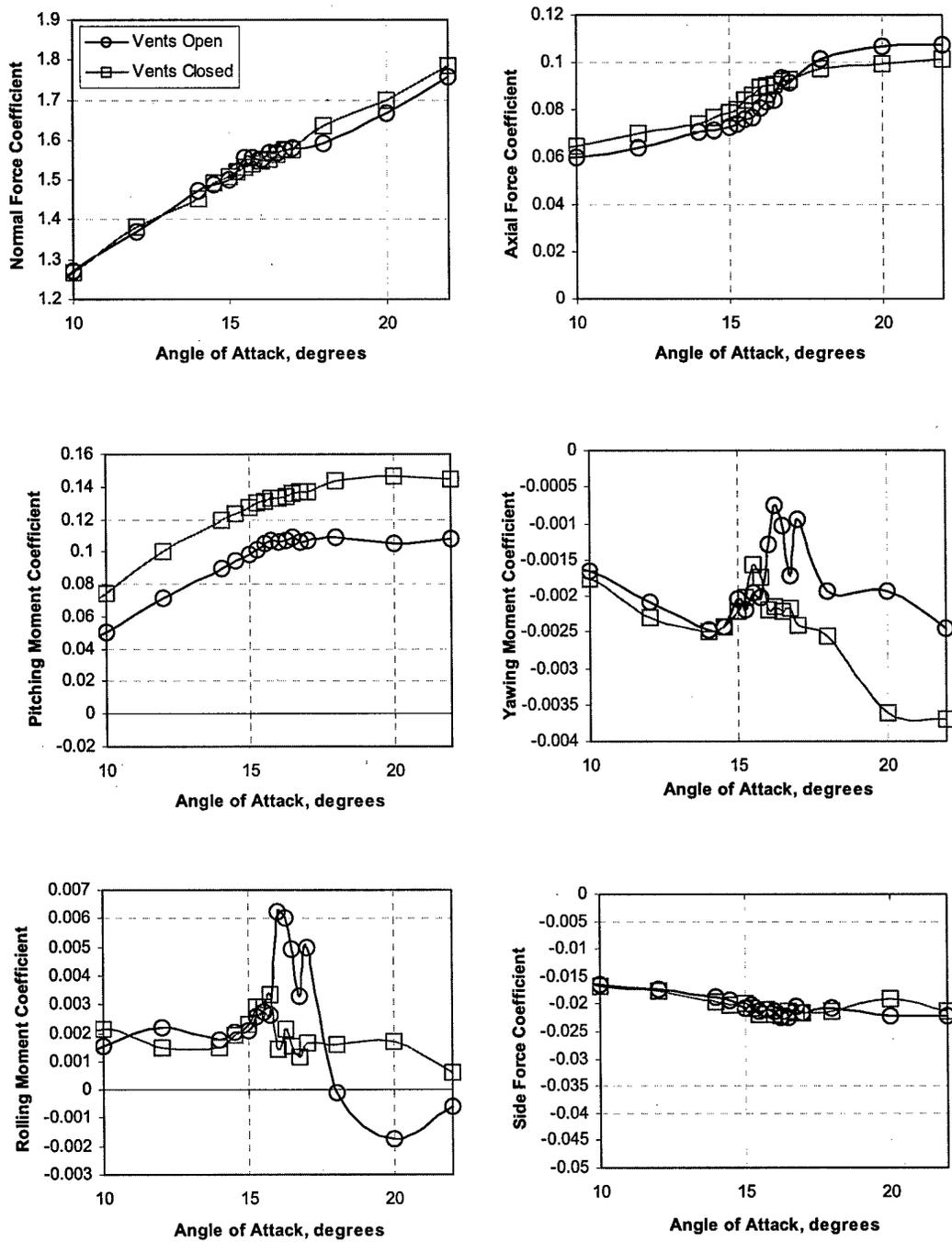
Figure 3-5: Angle of Attack vs. Force and Moment Coefficients, Comparison Between Vents Open and Vents Closed, Static Data

24

Sideslip angle (Beta) sweeps characterize the static lateral stability, which is known to affect the frequency of wing drop oscillations. Figure 3-6a shows the sideslip versus rolling moment coefficient curves for several values of angle of attack for vents closed configuration.
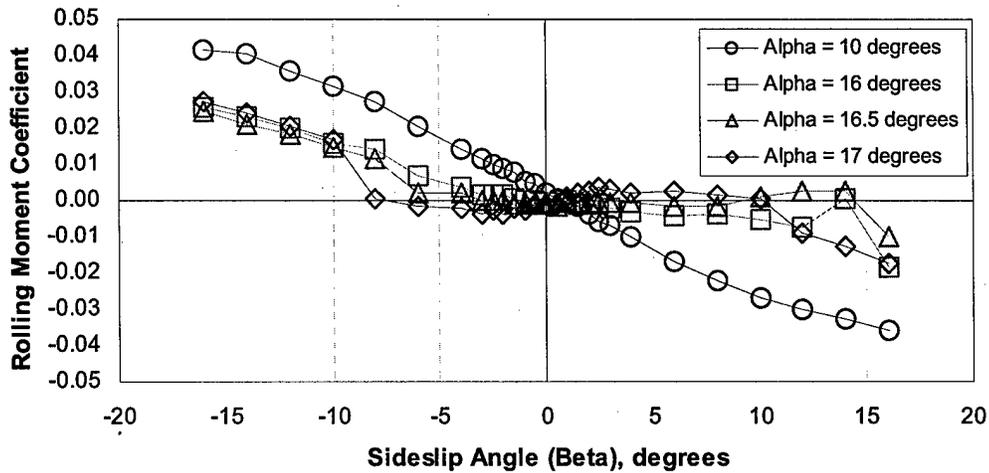
(a) Vents Closed
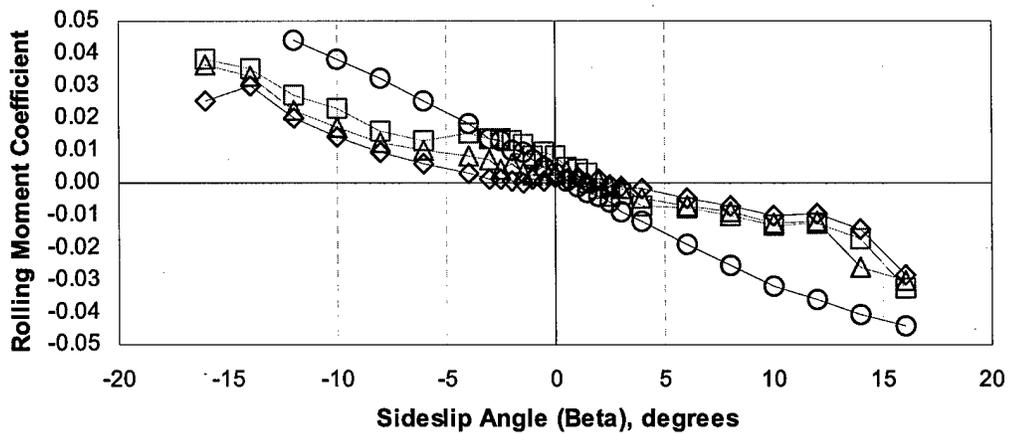
(b) Vents Open

Figure 3-6 (a, b): Static Lateral Stability Plot (Sideslip vs. Rolling Moment Coefficient), Static Data.

As expected the curve for 10° angle of attack shows stable static lateral stability. At the higher angles of attack the curves start to flatten out indicating some neutral stability.

This occurs primarily between –5° and 5° sideslip. This correlates with the range mentioned earlier. At 17° the curve starts to slope somewhat in the positive direction indicating static lateral instability. Figure 3-6b shows the vents open configuration results for the static lateral stability. For 10° and 16° angle of attack the curve has a strong negative slope indicating stability. The two other curves have slightly neutral stability. This information indicates that there is a change in the stability when the vents are open for 16° angle of attack. It changes from neutral to strong stable.

3.1.3 Correlation to Previous Tests

The static results discussed above indicate that angles of attack 14.5°, 15.5°, and 16.5° are critical states based on the reflex in the lift curve slope and the other static force and moment curves. This is consistent with the findings of Cook [3] and Niewoehner [5].

3.1.4 Hysterisis

A handful of runs were conducted to look at the effects of hysterisis. Figure 3-7 shows a time history for rolling moment coefficient with a continuous beta sweep at 10° angle of attack. The blue line shows that over a period of 80 seconds, as indicated on the x-axis, the sideslip angle was continuously swept from –16° to 16°. The red line also shows a continuous sideslip sweep over 80 seconds, starting at 16° and decreasing to –16°. At this angle of attack there is no strong evidence of hysterisis.
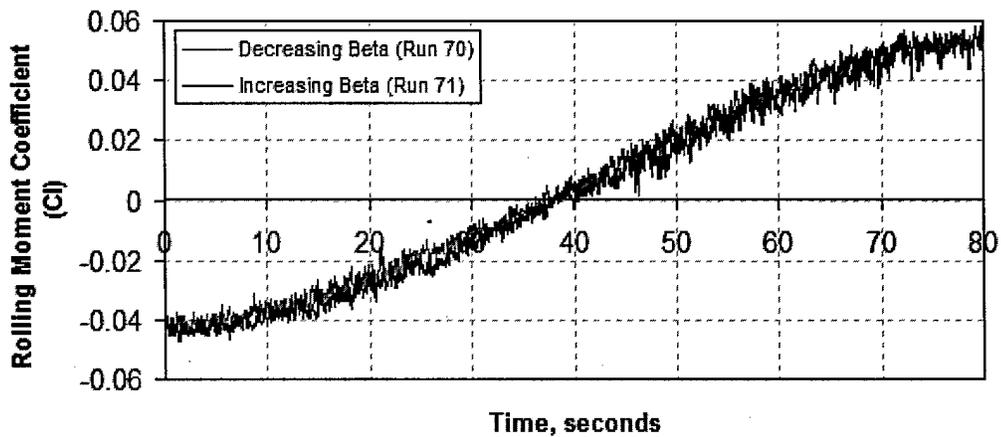
Figure 3-7: Rolling Moment Coefficient Hysterisis Analysis at 10° Angle of Attack, Static Data

On the other hand Figure 3-8, which depicts the same information but for 16.5° angle of attack, shows that at the larger negative values for beta there is some hysterisis effect. Since the beta range of this study is approximately -5° to 5°, this effect is negligible.
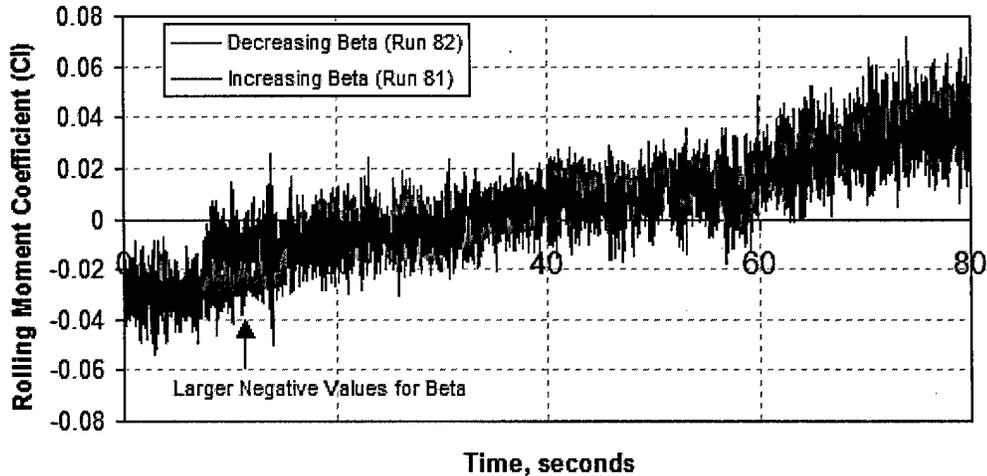

Figure 3-8: Rolling Moment Coefficient Hysterisis Analysis at 16.5° Angle of Attack, Static Data

3.1.5 Information Gained for Free-to-Roll Test

The results from the static force and moment test established a focus for the FTR testing about the critical state of 16° angle of attack.

3.2 Free-to-Roll Test Results

3.2.1 Results from the Continuous Pitch Sweeps

The continuous pitch sweep points were designed to yield a range of alpha at which there was a potential for wing drop. Due to the data acquisition limitations the values for the angle of attack and the pitch angle were not recorded. Figure 3-9 shows the roll angle time history for the vents closed PA-half configuration. The blue line indicates the roll angle value as the pitch angle is increased from 4° to 22° with time. While the red line shows the roll angle as the pitch angle is decreased from 22° to 4° with increasing time. Both points were taken after the wings were initially level. The pitch angle ranges from 12° to approximately 18° over a 15 second period of time between 20 and 35 seconds. This plot shows that during this portion of time there are clear variations in the roll angle consistent with a wing drop. The plot also shows that the effects of hysterisis are minimal.
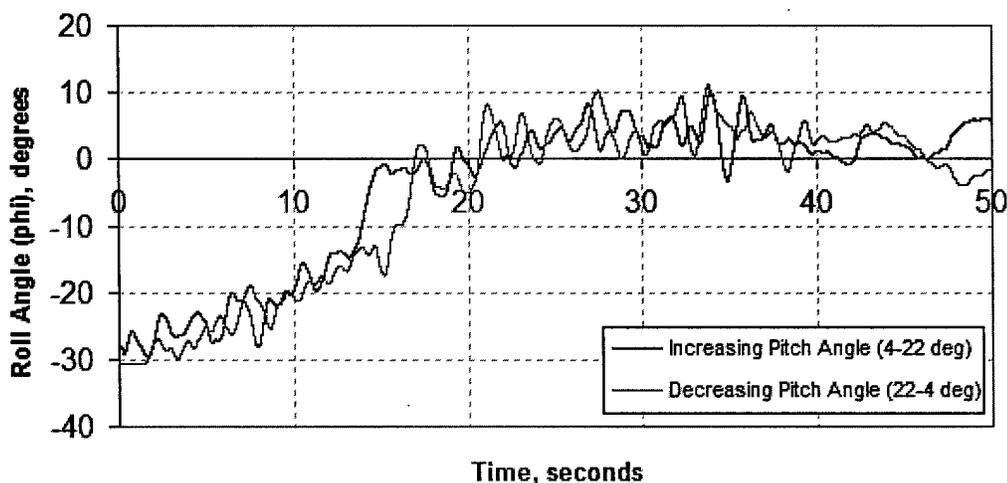

Figure 3-9: Roll Angle Time History for Continuous Pitch Point, FTR Data

28

3.2.2 Results from the Bank and Release Test Points

The System Identification Programs for Aircraft (SIDPAC) tool was used to calculate roll damping from the FTR data. The roll angle data was differentiated twice to determine the roll rate and acceleration. Referring back to the equation of motion,

$$\frac{I_x \ddot{\phi}}{qSb} + C_{l\dot{\phi}} \frac{\dot{\phi} b}{2V_\infty} + C_{l\phi}\phi = C_{lo},$$ the only unknowns are $C_{l\dot{\phi}}, C_{l\phi}$, and C_{lo}. The SIDPAC

method computes these aerodynamic terms by using a least squares estimate of the known real parameters. Bryant et al. discussed the results of this process and concluded that roll damping did not propel the wing drop observed in this study [2]. Figure 3-10 shows that the roll damping coefficient values are negative for all angles of attack shown - indicating stable roll damping.
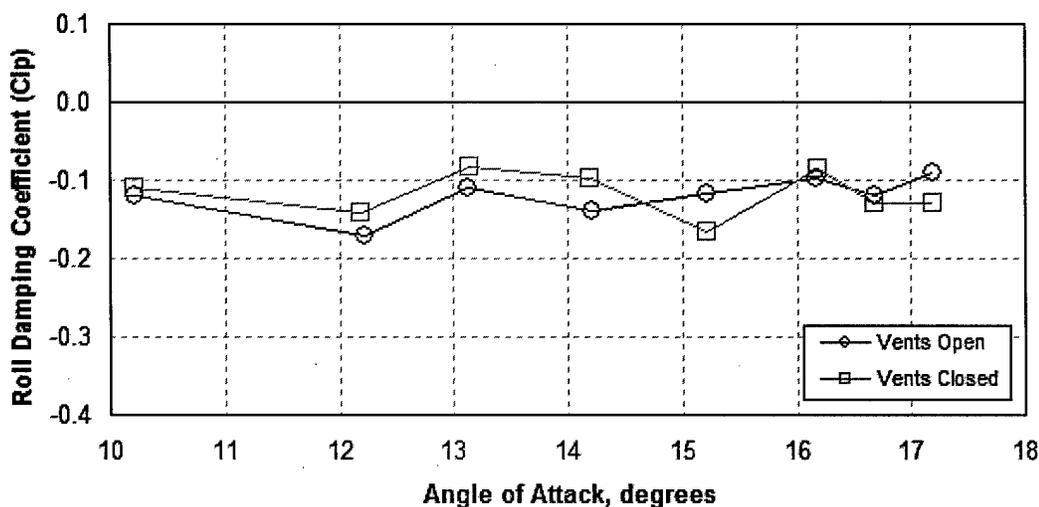

Figure 3-10: Roll Damping Effects [2], FTR Data

29

3.2.3 Results from the Pitch Pause Points

The pitch pause points provided information on the lateral activity at specific pitch angles. When the wings are level these pitch angles correspond to angles of attack. The FOM values were calculated for various angles of attack for both the vents open and closed configuration. Figure 3-11 shows the results and is divided into several ranges and regions for discussion purposes.
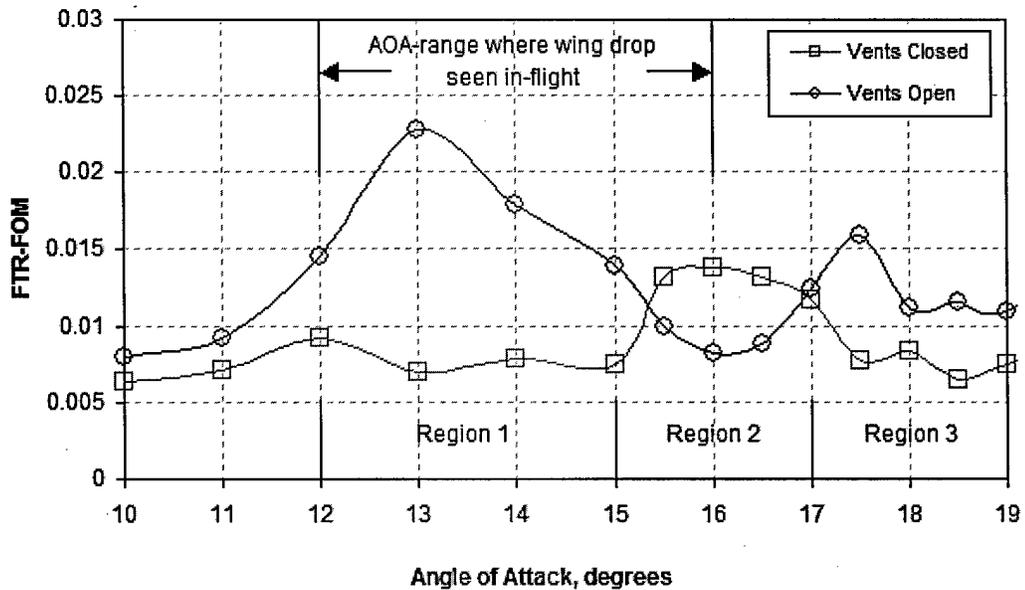
Figure 3-11: FTR-FOM [2]

The top range indicates the angles of attack at which the wing drop was experienced in flight. Region 1 exhibited higher FOM values for the vents open configuration than for the vents closed configuration. Intuitively based on previous wind tunnel tests, including the present test, this was unexpected since those tests indicated that there was no lateral activity or wing drop at the lower angles of attack. On the other hand the pre-production flight tests did report wing drop at angles of attack as low as 12°. This means that the FTR test captured the lateral motion at lower angles of attack not previously recorded by

static tests or CFD. In Region 2 the results were mixed. At 15.5°, 16°, 16.25 and 16.75° angle of attack the FOM values were higher for vents closed than open. Since a higher FOM means more lateral activity these results did not match those of the indicators in the static tests. Further investigation into the results from both the static and the FTR tests was needed to explain the increased lateral motion for the vents closed configuration. An in-depth analysis was conducted on 13° angle of attack from Region 1, 16° angle of attack from Region 2, and 15° angle of attack was analyzed as a transition between the two aforementioned Regions. No angles of attack were analyzed from Region 3 because they fall outside the range where the problem was seen in flight and in previous tests.

3.3 Analysis of Results for Specific Angles of Attack

3.3.1 Methodology

Three angles of attack were analyzed in the same manner to determine the cause of the lateral motion for their respective configurations. First the roll angle time histories from the FTR tests were analyzed to reinforce the results from the FTR-FOM plot. The remainder of the causal investigation into the lateral motion focused around the equation of motion: $\dfrac{I_x \ddot{\phi}}{qSb} + C_{l\dot{\phi}} \dfrac{\dot{\phi} b}{2V_\infty} + C_{l\phi}\phi = C_{lo}$. There were three possible contributors to the lateral motion or wing drop seen in each case. The first was the existence of an aerodynamic forcing function (right hand side of equation) and its nature. The nature of the function could be steady or unsteady. An unsteady forcing function with enough amplitude and low enough frequency could contribute to lateral motion or wing drop. The nature and existence of the forcing function was investigated via the time-averaged

rolling moment coefficient values for the specific angles of attack and via the time histories from this static data.

The second possible contributor was the spring effect (restoring force) represented by the static lateral stability (C_{l_ϕ}). This is the third term on the left hand side of the equation.

The character of the spring: stable, neutrally stable, or unstable, provided conditions under which a forcing function could react. The information on the character was gathered from the static force and moment data.

The last possible contributor from the equation of motion is the roll damping (second term on left hand side). Based on the results from **Section 3.2.2** it was concluded that the roll damping was not a significant contributor to the lateral motion and therefore is it will not be detailed in this section.

3.3.2 Region 1: Angle of Attack =13°

The first point of interest was 13° angle of attack. This value exhibited the largest difference in FOM value between the vents open and the vents closed configuration. Figure 3-12 shows the FTR roll angle time history for the two configurations at 13° angle of attack. The plot shows that the vents open configuration had aperiodic spikes with a significant amount of amplitude, when compared to the small amplitudes exhibited by the vents closed. These larger amplitude spikes contributed to the higher FOM values for the vents open and therefore confirmed the results from Figure 3-11. Hence closing the vents decreased the motion at 13°angle of attack.

32
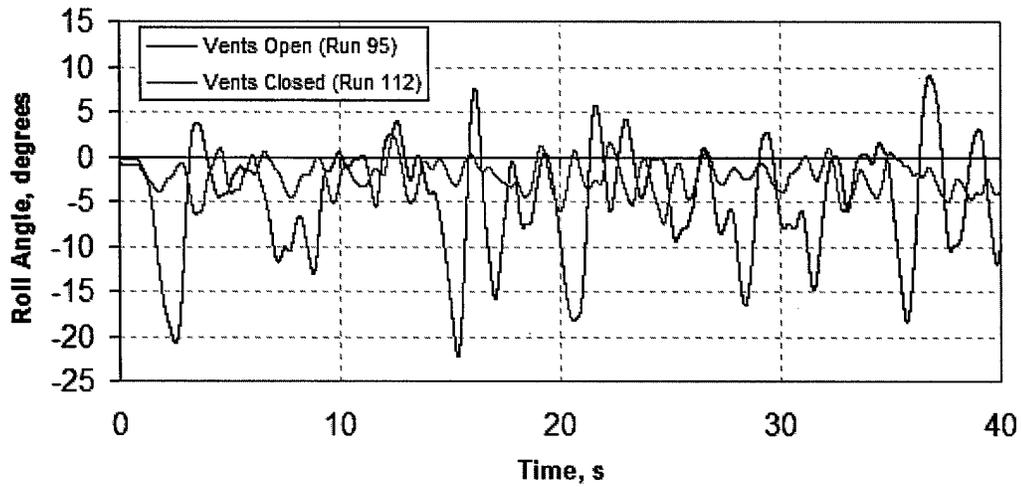
Figure 3-12: Lateral Motion Analysis for Vents Open and Vents Closed, Angle of Attack 13°, FTR

Data

The first possible contributor to the lateral motion is the forcing function contribution. Figure 3-13 shows the time-averaged static rolling moment for a range of alpha. As noted by Bryant et al. there is an average offset of 0.002 for the two configurations. This offset can be the result of either model asymmetries and or tunnel sidewash [2]. The data will be analyzed relative to the offset.


Figure 3-13: Time-Averaged Static Rolling Moment, Static Data

33
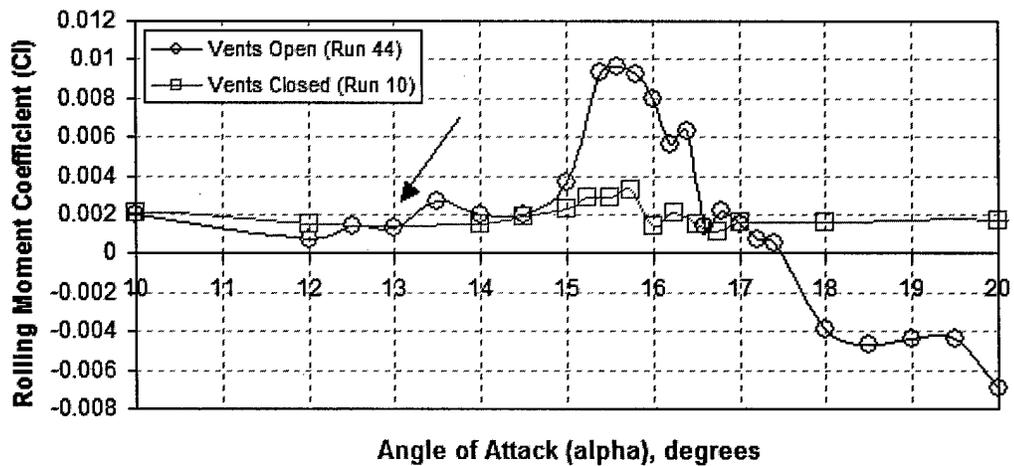
At 13° angle of attack the vents open curve shows no significant jump or spike indicative of a critical state or forcing function. Although there is no actual test point at 13° for vents closed, it is assumed that the character of the line is similar throughout; therefore there is also no indication of a critical state or forcing function for vents closed. Since the information in Figure 3-13 is time-averaged a closer look at the time histories for this data revealed that there is a forcing function for both configurations. Figure 3-14 shows the rolling moment balance time history for the two configurations at 12° angle of attack. Data was not available for the vents closed configuration at 13° therefore 12° was chosen to be representative of the Region 1 data. From Figure 3-14 it is clear that the vents open curve exhibits an unsteady forcing function characterized by sharp aperiodic spikes. These spikes had enough amplitude at low enough frequency to produce rigid body motion.
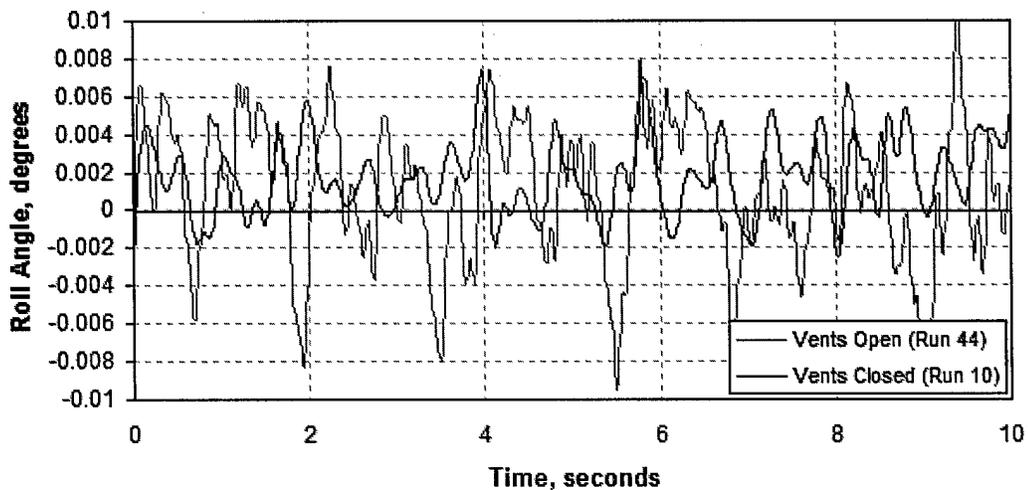

Figure 3-14: Rolling Moment Time Histories at Angle of Attack 12°, Static Data

The second contributor was the static lateral stability or spring effect. Given the absence of information for the vents closed at 13°, Figure 3-15 shows the spring effect for vents open at 13°. The steep negative slope indicated that the restoring force is strong and stable.
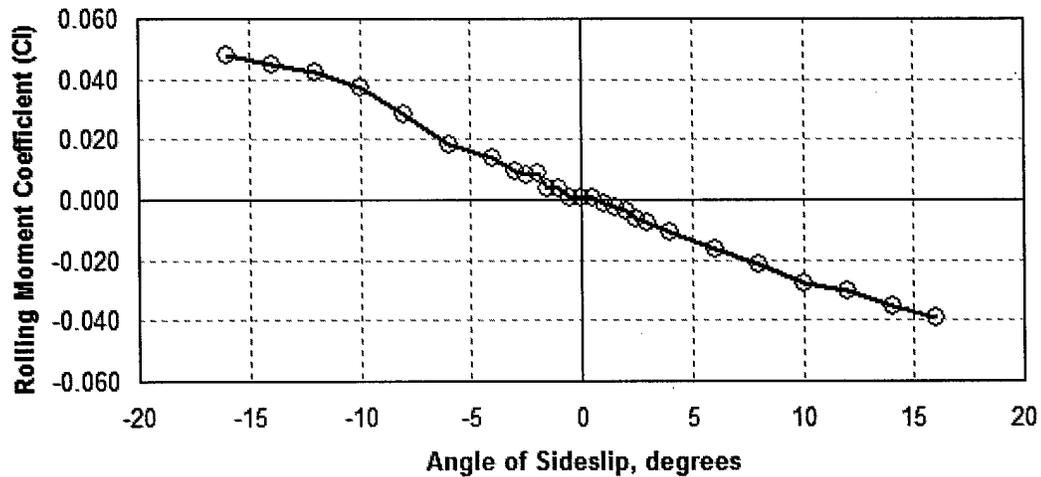

Figure 3-15: Static Lateral Stability for Vents Open Configuration, Angle of Attack 13°, Static Data

The restoring force had the ability to return the model to a wings level position after it had been disturbed by the forcing function, hence the large amplitude spikes in Figure3-12 and the higher FOM values for vents open. The results attributed the increased lateral activity experienced at 13° angle of attack, vents open, to an unsteady forcing function and a strong stable spring.

3.3.3 Transition Between Regions 1 and 2: Angle of Attack =15°

The second point analyzed was 15° angle of attack, representative of a transition point between Regions 1 and 2. This point was of interest because wing drop was experienced at this angle of attack in pre-production flight tests. Although the difference in FOM value between the two configurations was smaller than at 13°, the vents open

configuration maintained a higher FOM value than the vents closed. The roll angle time history for both configurations is depicted in Figure 3-16. The blue line for the vents open configuration indicated some sinusoidal motion characterized by several large amplitude spikes. In comparison the vents closed configuration had much smaller values of amplitude. These characteristics were consistent with the results from the FTR-FOM plot (Figure 3-11), which indicated that the vents open had a larger FOM value.
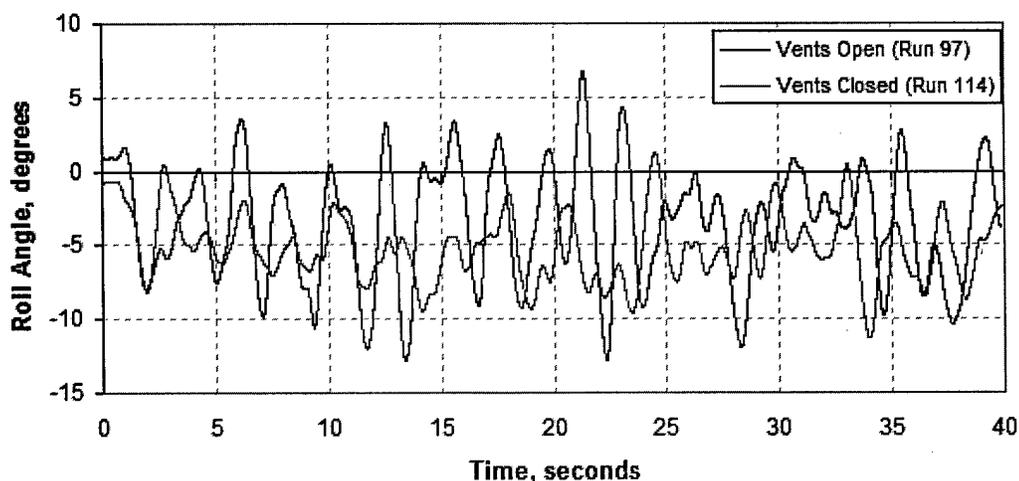

Figure 3-16: Roll Angle Time History for Angle of Attack 15°, FTR Data

Focusing on the first possible lateral motion contributor, a forcing function, Figure 3-13 was reinserted for reference (Refer to **Section 3.3.2** for offset explanation). At 15° angle of attack the time-averaged rolling moment coefficient for the vents open configuration is about 0.002 higher than the vents closed configuration. The vents open curve has a distinct increase in slope at this angle indicative of the potential for some increased lateral motion. This change in slope of the aerodynamic parameter is an indication of a bifurcation as discussed by Cook [3].

36

The vents closed configuration does not show a significant spike or change in slope. Based on this information there is some indication of a forcing function for the vents open configuration, but not for the vents closed configuration.
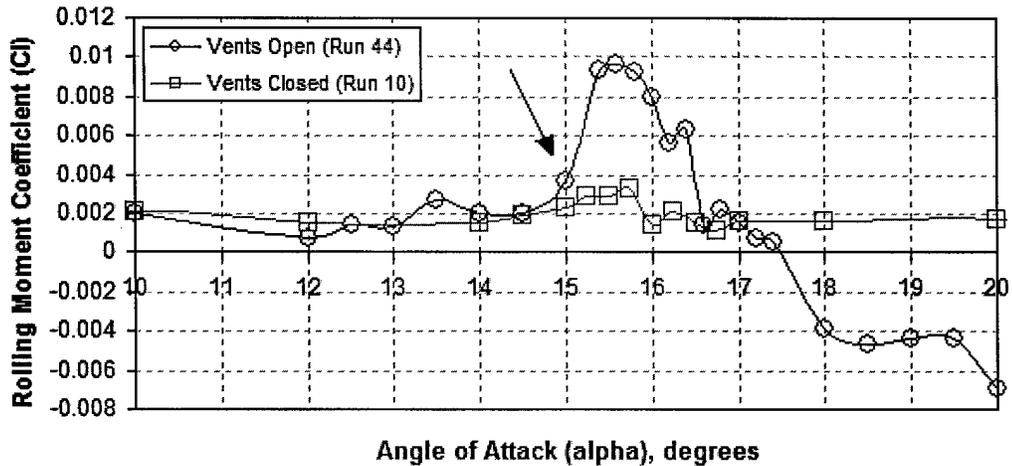

Figure 3-13: Time-averaged Static Rolling Moment, Static Data

Further investigation of the time-averaged data via the static rolling moment coefficient time histories is shown in Figure 3-17. Figure 3-17 shows that both configurations had unsteady forcing functions with enough change in rolling moment coefficient to cause significant lateral motion with the vent open having the largest change.
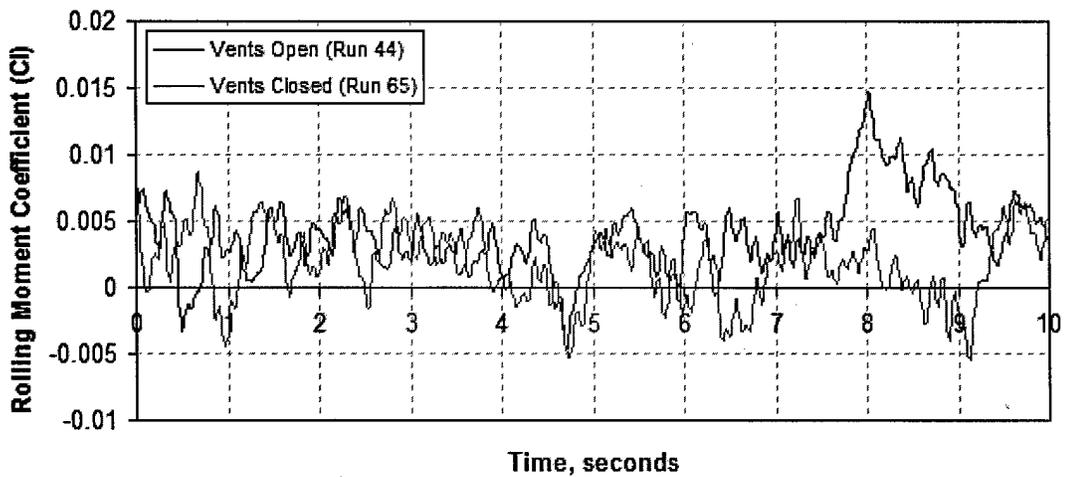

Figure 3-17: Rolling Moment Coefficient Time Histories for Angle of Attack 15°, Static Data

The second possible lateral motion contributor, the static lateral stability, is investigated via Figure 3-18. The figure shows the static lateral stability curve for the vents open configuration for 15° angle of attack. There was no data available for the vents closed configuration. The static stability curve is nonlinear with several changes in the stability. From –4° to 6° the spring force is strong stable, with nonlinearities at –1° and 4°. The strong positive spring and an unsteady forcing function could cause the increased lateral motion for the vents open configuration, similar to that seen for 13° angle of attack.
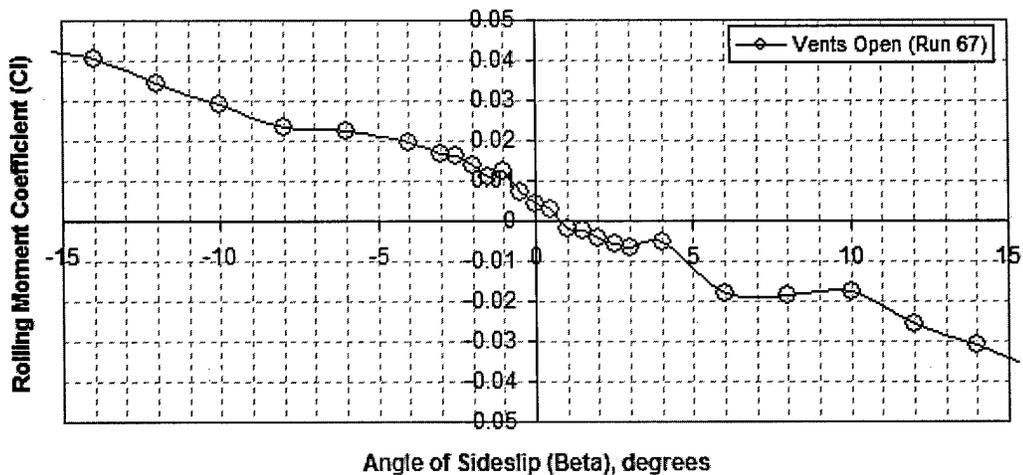

Figure 3-18: Static Lateral Stability for Angle of Attack 15°, Static Data.

The nonlinearities were of concern, but no duplicate runs were done for these conditions in order to further investigate the cause. A plot of the sideslip angle time history corresponding to the FTR data, Figure 3-19, indicates that for this particular configuration the range of sideslip angle is approximately –3° to 2°. Based on this range the nonlinearity at –1° remained of concern.
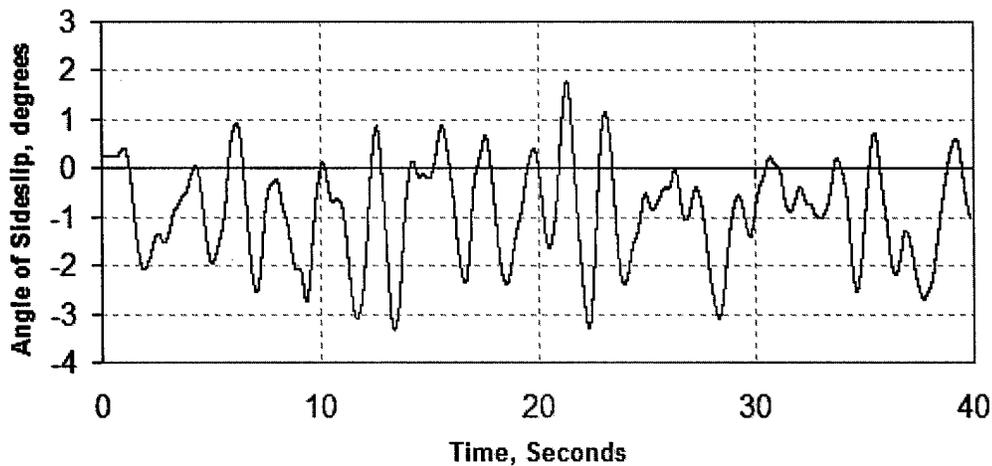
Figure 3-19: Angle of Sideslip Time History for Angle of Attack 15°, FTR Data.

The possible contributors to the increased lateral motion at 15° angle of attack for the vents open configuration were the unsteady forcing function and the strong stable static lateral stability.

3.3.4 Region 2: Angle of Attack=16°

This point was of interest because it was on the high end of the in flight range and it was identified by the static and CFD tests as a critical state. In addition, this point has a higher FOM value for the vents closed configuration than for the vents open. The roll angle time history from the FTR data, Figure 3-20, reflects the difference in FTR-FOM value. The vents closed configuration exhibits large sinusoidal lateral motions with a left wing down bias. This contradicts the information in Figure 3-13, which indicates a right wing bias. It appears that the change from the static mount to the FTR rig induced a left wing stall tendency seen in Cook's study [3]. Fortunately this study was intended to investigate the lateral motion tendencies and not to predict specific aircraft motions.
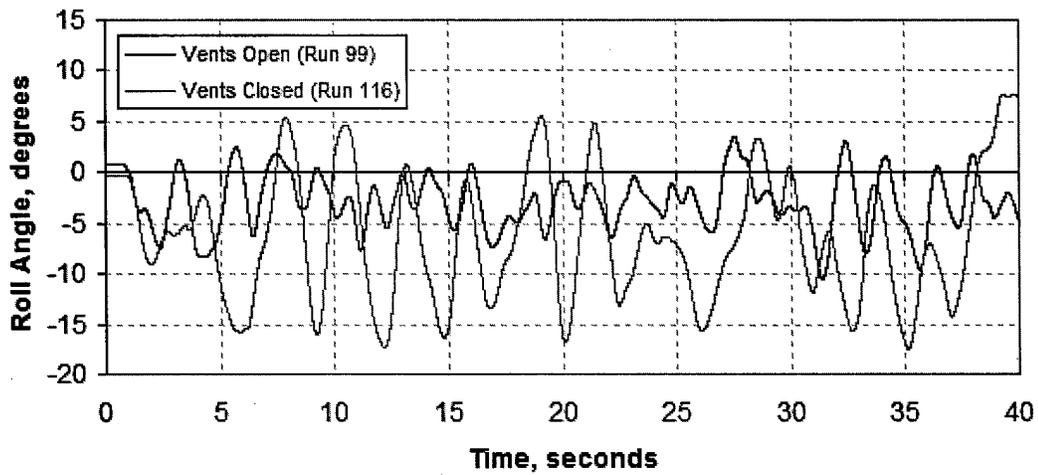
Figure 3-20: Roll Angle Time History for Angle of Attack 16°, FTR Data

Considering the existence of a forcing function as a possible contributor to the lateral motion, Figure 3-13 is reinserted as a reference (Refer to **Section 3.3.2** for offset explanation). The plot indicates that at 16° there is a distinct change in the slope of the vents open configuration. This is a flag to the possibility of a critical state where wing drop might occur.
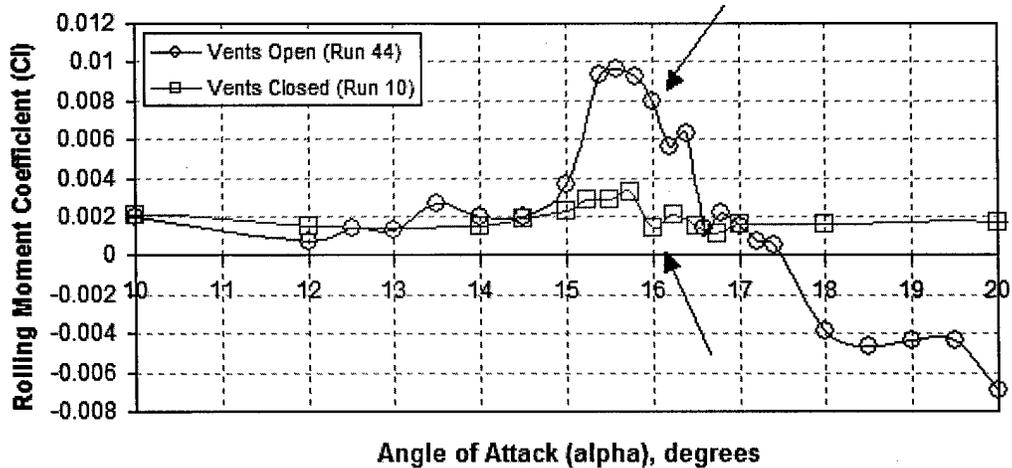

Figure 3-13: Time-Averaged Static Rolling Moment Coefficient, Static Data

40

Based on Figure 3-13 the vents open configuration exhibits a forcing function. Looking at the static rolling moment coefficient time history from the time-averaged data, Figure 3-21, reveals the existence of a forcing function for both the vents open and the vents closed configuration. Although both configurations exhibited an unsteady forcing function of significant amplitude, the lower frequency variations for vents closed made it a more likely contributor to the rigid body motion.
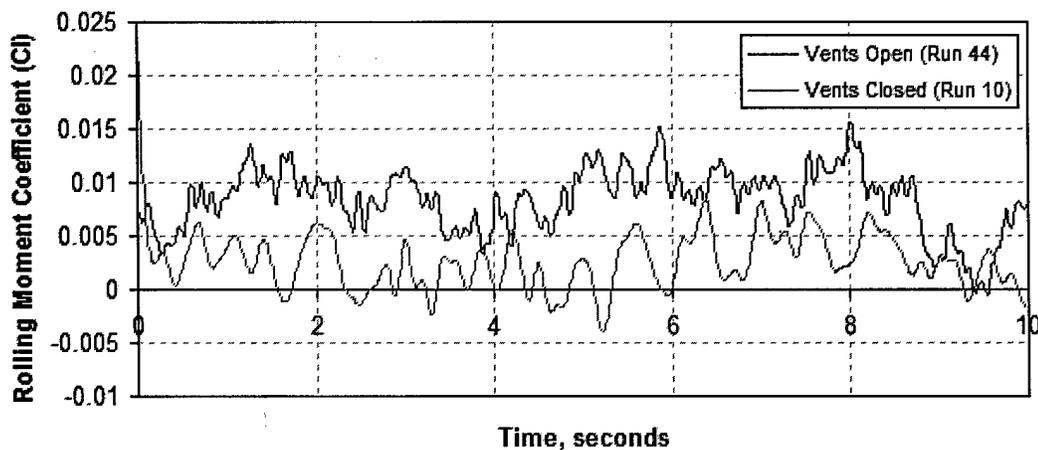

Figure 3-21: Rolling Moment Coefficient Time History

To assess the other possible cause of the rigid body motion the static lateral stability is plotted in Figure 3-22. The static lateral stability for 16° angle of attack shows that the vents closed configuration had neutral stability between −5° and 5° beta. In other words, there is no restoring force in this range. Therefore the model tended to roll back and forth through this beta range until a restoring force could counteract the unsteady forcing function shown in figure 3-21. The vents open configuration had a strong restoring force and a higher frequency forcing function that confined the lateral activity to smaller amplitudes, hence the lower FTR-FOM value.
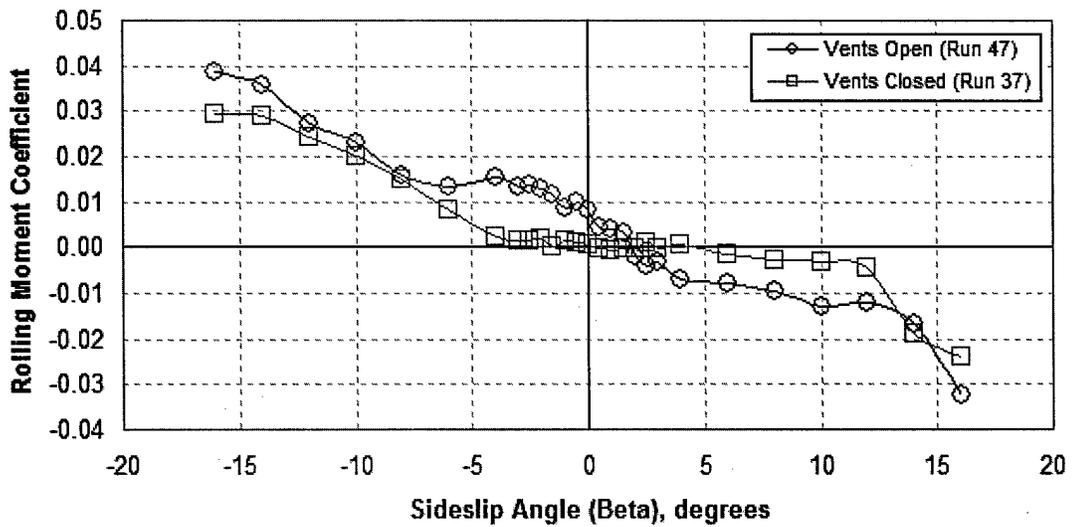
Figure 3-22: Beta vs. Rolling Moment Coefficient for Angle of Attack 16°, Static Data

Figure 3-23 shows that the beta range over which the model traversed during the FTR test was −3° to 1° for the vents open configuration and −5° to 2° for the vents closed configuration. Both of these ranges are well with in the −5° to 5° shown in Figure 3-22.
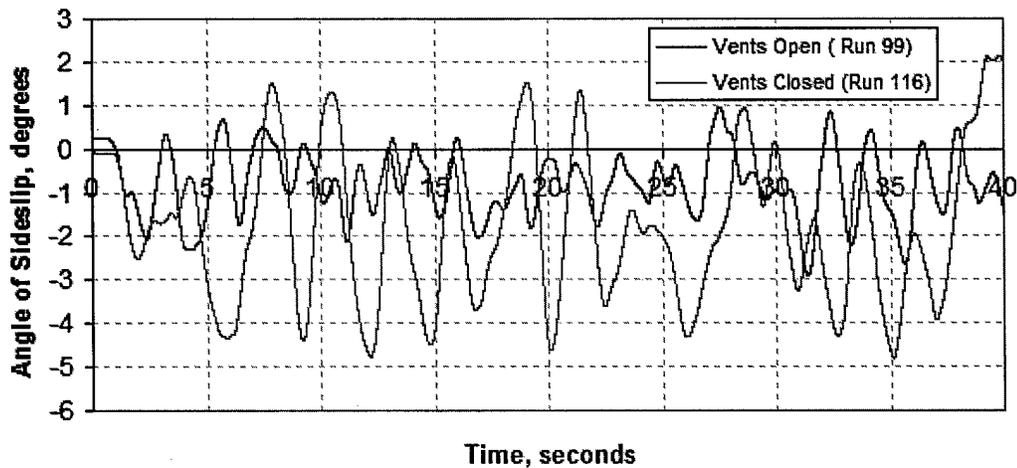
Figure 3-23: Angle of Sideslip Time History for Angle of Attack 16°, FTR Data

The cause of the lateral motion and therefore increased FOM value for vents open was the neutral static stability and the unsteady forcing function with enough amplitude and

low enough frequency to perpetuate the rolling motion. On the other hand, although vents closed had a strong stable spring, the frequency of the unsteady forcing function was high enough that it did not cause as much lateral motion as the vents open

4 Conclusions

This study proved to be a valuable asset in advancing the use of FTR in the determination of subsonic wing drop potential in pre-production models, namely the F/A-18E. All the objectives including correlation to previous tests, lateral motion assessment, and feasibility determination were accomplished.

4.1 Correlation

The static force and moment test results correlated with the previous static tests and CFD analysis, which identified a critical state at approximately 16° angle of attack. When combined with the static test results the FTR results proved to be invaluable in the determination of wing drop potential, because they captured the α-range where wing drop was seen in flight. This is significant in the determination of feasibility because the previous tests were unable to capture the lower range.

4.2 Lateral Motion Assessment

From the analysis conducted it was clear that there were a couple contributors to the lateral motion identified by the FTR-FOM. The equation of motion pointed to the forcing function and the static lateral stability. There were different results for various ranges of angle of attack. In Region 1 the increased lateral activity experienced at 13° angle of attack, vents open, was a product of the unsteady forcing function and a strong spring force. Possible contributors to the increased lateral motion at 15° angle of attack, vents open, were the unsteady forcing function and the strong stable static lateral stability. In Region 2 the vents closed lateral activity for vents closed at 16° was

attributed to an unsteady forcing function and a neutrally stable spring. The smaller amount of motion for vents open was a consequence of the high frequency forcing function and the strong stable spring. The roll damping did not propel the motion for any of the points analyzed.

4.3 Feasibility

Using a FOM the FTR test technique proved to be feasible in determining the potential for uncommanded lateral motions at subsonic speeds for the pre-production F/A-18E. Since the static data did not indicate the potential for wing drop (critical states) at the lower angles of attack, the importance of using the FTR test technique is emphasized along with the fact that neither set of data is stand alone.

4.4 Future Endeavors

Follow on research in this area should include:

- Additional static and FTR tests within a larger angle of attack range with smaller increments for both the vents open and closed configurations. The goal is to further investigate the points discussed in this study and expand upon others.

- Force oscillation study to determine the any additional roll damping considerations.

Bibliography

[1]   Anderson, J.D. <u>Fundamentals of Aerodynamics</u>. Second Ed., McGraw-Hill Inc. New York, 1991.

[2]   Bryant, E.M., Owens, D.B., Barlow, J.B. "Free-To-Roll Investigation of Uncommanded Lateral Motions for an Aircraft with Vented Strakes," AIAA-2005-0239, January 2005.

[3]   Cook, S., "On Flow Topology Changes Accompanying Aerodynamic Bifurcation for Aircraft with Vented Strakes", Ph.D. Dissertation, University of Maryland, 2003.

[4]   Ericsson, L.E. "Various Sources of Wing Rock," *Journal of Aircraft*, Vol.27, No. 6, 1990.

[5]   Filbey, J., Niewoehner, R. "A Computational Study of F/A-18 Wing Drop in the Approach Configuration," AIAA-2001-4194, August 2001.

[6]   Internet Website: "F/A-18 Hornet," http://danshistory.com/fa18.html

[7]   Internet Website," F/A-18 Background Info," http://www.boeing.com/defense-space/military/fa18/fa18_4back.htm

[8]   Internet Website, "The World of Bifurcation,"

        http://www.bifurcation.de/

[9]   Owens, D. B., Capone, F.J., Hall, Brandon, J. M., Cunningham, K.

        "Free-To-Roll Analysis of Abrupt Wing Stall on Military Aircraft at

        Transonic Speeds," AIAA-2003-0750, January 2003.

[10]   Raj, P., Finley, D. B., Ghaffari, F. "An Assessment of CFD

        Effectiveness for Vortex-Flow Simulation to Meet Preliminary Design

        Needs," Research and Technology Agency, MP-69-P-47, May 2001.

[11]   Rom, J. High Angle of Attack Aerodynamics: Subsonic, Transonic, and

        supersonic Flows, Springer-Verlag, New York, 1992.

[12]   Wolowicz, C.H. "Similitude Requirements and Scaling Relationships as

        Applied to Model Testing," NASA Technical Paper 1435, 1979.